ISSN 8755-6839

SCIENCE OF **TSUNAMI HAZARDS**

Journal of Tsunami Society International

Volume 34 **Number 4** **2015**

** (Note: Based on the Field Survey Report of the tsunami effects caused by the August 2012 Earthquake compiled in a report by international participants.)*

WWW.TSUNAMISOCIETY.ORG

TSUNAMI SOCIETY INTERNATIONAL, 1741 Ala Moana Blvd. #70, Honolulu, HI 96815, USA.

SCIENCE OF TSUNAMI HAZARDS is a CERTIFIED OPEN ACCESS Journal included in the prestigious international academic journal database DOAJ, maintained by the University of Lund in Sweden with the support of the European Union. SCIENCE OF TSUNAMI HAZARDS is also preserved, archived and disseminated by the National Library, The Hague, NETHERLANDS, the Library of Congress, Washington D.C., USA, the Electronic Library of Los Alamos, National Laboratory, New Mexico, USA, the EBSCO Publishing databases and ELSEVIER Publishing in Amsterdam. The vast dissemination gives the journal additional global exposure and readership in 90% of the academic institutions worldwide, including nation-wide access to databases in more than 70 countries.

OBJECTIVE: Tsunami Society International publishes this interdisciplinary journal to increase and disseminate knowledge about tsunamis and their hazards.

DISCLAIMER: Although the articles in SCIENCE OF TSUNAMI HAZARDS have been technically reviewed by peers, Tsunami Society International is not responsible for the veracity of any statement, opinion or consequences.

Submit manuscripts of research papers, notes or letters to the Editor. If a research paper is accepted for publication the author(s) must submit a scan-ready manuscript, a Doc, TeX or a PDF file in the journal format. Issues of the journal are published electronically in PDF format. There is a minimal publication fee for authors who are members of Tsunami Society International for three years and slightly higher for non-members. Tsunami Society International members are notified by e-mail when a new issue is available. Permission to use figures, tables and brief excerpts from this journal in scientific and educational works is granted provided that the source is acknowledged.

Recent and all past journal issues are available at: http://www.TsunamiSociety.org CD-ROMs of past volumes may be purchased by contacting Tsunami Society International at postmaster@tsunamisociety.org Issues of the journal from 1982 thru 2005 are also available in PDF format at the U.S. Los Alamos National Laboratory Library http://epubs.lanl.gov/tsunami/

ISSN 8755-6839

SCIENCE OF TSUNAMI HAZARDS

Journal of Tsunami Society International

Volume 34 Number 4 2015

THE INEXPENSIVE DEVICE FOR SEA LEVEL MEASUREMENTS

A. Annunziato

EC-Joint Research Centre (EC-JRC), Italy

ABSTRACT

A new mareograph device has been designed at the Joint Research Centre (JRC) of the European Commission (EC) in order improve the sea level network in use for the Tsunami Hazard monitoring in the Mediterranean Sea and in the North Atlantic area (NEAMTWS area of UNESCO). The instrument has the characteristic to be cheap and very effective but its reliability, duration and quality need to be determined and qualified. For this reason a number of experimental campaigns are being conducted, whose first results are presented here. In collaboration with the UNESCO/IOC (Intergovernmental Oceanographic Commission), responsible of the definition of the Tsunami Warning System of this geographical area, a set of 20 devices has been offered by JRC for a period of 1 year of testing of the devices; the surveys for the installation of the devices is under way and the installation should be completed by the end of 2015.

Keywords: *Early Warning Systems, Tsunami, and Sea Level Measurements*

Vol. 34, No. 4, page 199 (2015)

1. INTRODUCTION

The Mediterranean Sea, Black Sea and North Atlantic areas have been subject over the history to a number of devastating Tsunamis (Crete -365, Lisbon 1755 just to indicate the major events). The Inter-Governmental Oceanographic Commission (IOC) of UNESCO is therefore developing the Tsunami Warning System for this region since 2004, as a result of the international efforts after the Sumatra event.

Figure 1 – Tidal Gauges Instruments in the Mediterranean Sea, Black Sea and North Atlantic Ocean

At the same time, meteorological important events may also occur in the area, causing Storm Surge and inundation when particularly severe wind/pressure conditions are present. In both cases monitoring the sea level is extremely important in order to be able to take decisions on what is the best control strategy.

Unfortunately, the sea level instrumentation is not at the same level of quality in the whole area (Figure 1) in terms of geographical distribution and quality of the measurements. For instance, the North African coasts lacks of instrumentation that would be extremely useful to monitor Tsunamis and to be able to take quick decisions or to monitor events with automatic systems like GDACS (Annunziato 2005, 2007, De Groeve et al 2007). Turkish coasts have only a few number of instruments. Italian, French and Spanish coasts are very well instrumented; some areas in the Adriatic Sea are poorly instrumented. UNESCO/IOC established a Task Group in order to monitor the installation of instruments and to rationalize their installation. Nevertheless, one challenge in

the diffusion of these instruments is their elevated initial and maintenance costs, their management and the quality of the measurements in terms of real time acquisition and data dissemination.

JRC installed 3 new mareographs in Greece in 2013. These are very advanced stations, containing 2 types of sensors (radar and pressure gauges), one high quality differential GPS antenna and an active data logger that transmits data to JRC and to NOA servers with few seconds' latency. The cost for the installation of these devices has been very high, including the installation and maintenance for 2 years.

A less complete but very effective station has then been installed in Portugal, Setubal, in order to serve the needs of the Tsunami Alerting Device, a last mile-alerting device developed by JRC that is being tested in Portugal. This device contains only a radar sensor and the data are transmitted to a local distant data collector via WI-FI transmitter and made continuously available to JRC to perform analyses and storage. The cost of this station has been 1/3 of the price of each station installed in Greece. Although this device was much less expensive than the ones installed in Greece, the large diffusion of devices is still prohibitive in terms of investment and maintenance costs. Therefore, JRC decided to create a low-cost mareograph prototype.

Based on the experience of other similar devices and the need during a Tsunami analysis, the requirements that we have fixed for the mareographs are the following:

• High quality of the data with an error of 0.5 cm maximum (sensitivity justified by the expected error in the sea level calculations)
• Short acquisition time interval, 15 s maximum (to have a well-defined sea level wave description over time)
• Small transmission latency, smaller than 30 s (this is particular important for small basins with low travel time)
• Low overall cost, less than 1.5 k€
• Autonomy, at least 3 days without solar irradiation (the autonomy can be increased to 7 days with an over cost and weight on the battery)

The prototype presented in this report costed about 1.2 k€, but the cost could be further reduced with proper selection and purchase of the material and if produced in large scale.

The heart of this device is the Raspberry Pi, which is a powerful electronic board that contains a Linux operating system with several standard components (USB, HDMI, Ethernet port, Video card, and sound card) and other busses that can easily be connected with external devices. The device therefore has a computer on which software can be installed and that can be reached remotely for debugging or software change. The other important component is the radar sensor: we have identified a relatively low cost rugged component that could be used as sea level sensor (after several tests presented in this report). Additional components are necessary in order to have an autonomous system (electrical power feed and communication). A name for the device that can capture the characteristics is IDSL, Inexpensive Device for Sea Level Measurements.

2. DESCRIPTION OF THE IDSL

2.1 The Hardware

The Inexpensive Device for Sea Level Measurement has been developed buying all standard easy to find components (see Figure 2), assembled in a compact plastic container box, with a second box containing power accumulators, needed when an autonomous installation has to be realized.

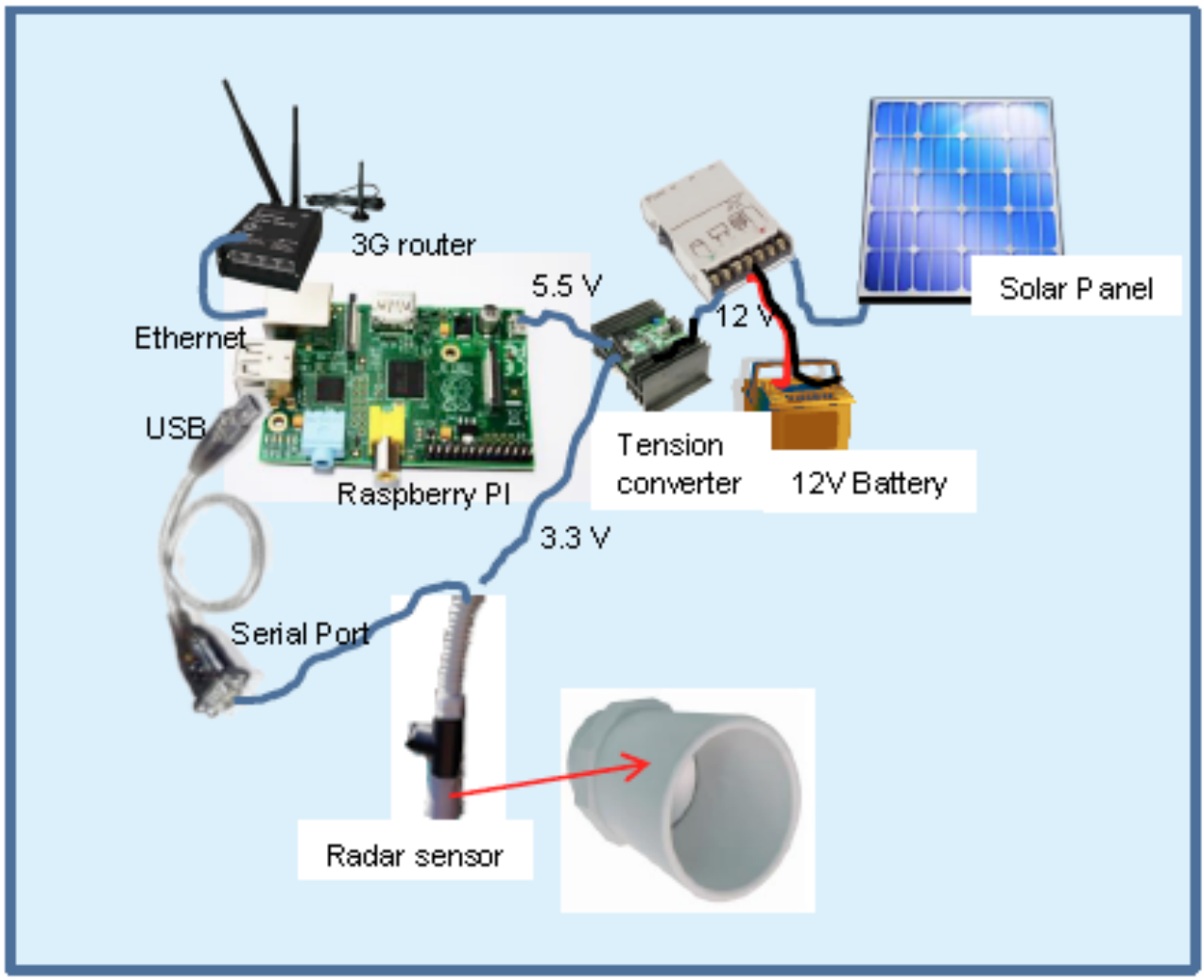

Figure 2 - Arrangement of the devices supporting the mareograph

A solar panel (100 W) is connected to a solar power regulator, needed to correctly charge the batteries; in case AC electrical power is available onsite, the regulator is fed by a voltage transformer of 13.5 V. The regulator is connected also with a small battery (7.2 AH), present in the first box. In case of AC power available this battery is used for potential temporary power failures with an autonomy of about 8 h. A second package containing additional 48 AH batteries can be connected to the first box in parallel to the 7.2AH battery.

The load section of the solar regulator feeds, through a voltage reducer, the computer/data logger, a Raspberry Pi B+ and directly the GSM modem. A Raspberry Pi is a very powerful small board (cost less than 35 euro) containing an ARM processor with Linux operating System, 4 USB ports, 1 Ethernet card and many I/O ports available to the user. The sea level sensor, a commercial radar device, is connected to the Raspberry using one of the available USB ports. The GSM modem is connected to the Raspberry using the local LAN offered by the GSM modem.

The solar panel takes energy and connects to a charge regulator. The regulator recharges the battery, when the panel voltage is within a certain range. In addition, it controls the output tension to the loads. When the battery discharges below a certain voltage (11 V) the loads are disconnected, until the battery goes back to more than 12 V (hysteresis). The output voltage from the regulator (12V) is sent to a voltage converter that reduces the voltage to 5.5 V (to feed the Raspberry) or 3.3 V (to feed the radar sensor).

The Raspberry receives input from the Radar sensor through an RS232 connection to one of its USB ports and transmits the data via a 3G router, connected with its Ethernet port.

In order to measure the battery and the panel tensions we use a voltage divider (to have a signal smaller than 5 V) and an Analog Digital Converter, applied on the Raspberry device (Figure 3). An external “watchdog” circuit is also included to make sure that, in case of irresponsive device for any reason a reset of the Raspberry is actuated. Additional devices present on the board are a temperature and a pressure sensor (pressure sensor only in the latest models).

The overall cost, also considering the metallic supports and the cost to assemble all the parts has been about 1.3 k€; no attempt to optimize the costs has been done and only off-the-shelf products have been adopted at retail prices. This means that a margin for cost reduction in case a large-scale production is performed, could be achieved.

Optimization of the power consumption is necessary due to the need to transmit continuously the data (every 5 s) and considering the power consumption of the various devices (2.5-3 W Raspberry, 3.5W GSM modem are the main sources). Therefore a combination of 100 W solar panel and 42.2 AH has been considered sufficient to keep on for at least 3 days a device installed at latitude 43.8 north.

2.2 The software

The control software of the device (the executable is named tad) is a single program started during the initialization phase of the operating system. In order to manage all the asynchronous operations, the program is multithreaded: this reduces the impact of lengthy operations on the overall responsiveness of the software.

At starting time, the control software reads its configuration, a set of named parameters in config.txt file, such as the USB port to access, the URL template to post the data to, or the parameters for the alert level calculation.

The sensor module is then started: it will start feeding the analysis module with the values provided by the sensors. Every sensor will write independently in a structure that contains all sensor data: water level, pressure, temperature, and battery charge, solar panel input.

At this point, the program is in an infinite loop, waiting for data to be processed. It will be stopped by a break signal or when the system shuts down. There is no way to alter the running configuration: in case of need, after changing the configuration file, the program must be restarted. It is possible to access remotely the Raspberry and act on the operating system.

The software pushes data into the JRC server every 5 seconds with a method developed by JRC and already applied to other sensors installed. A web service, present on the JRC Internet network allows to store the data; another software continuously monitor the presence of new data and stores them in the local SQL server database. All the data are therefore available at this web site: http://webcritech.jrc.ec.europa.eu/tad_server/?ID=64

The result of the Imperia experimental campaign (see later) allowed to debug, improve, optimize the software in order to keep alive as much as possible to application. For instance the automatic reboot of the Raspberry every 1h, then relaxed to 6h, has been found beneficial in terms of reliability and accumulation of error conditions from various sources.

3. RESULTS OF IMPERIA SEA LEVEL CAMPAIGN

As a result of a Collaboration Agreement between the Joint Research Centre and the Italian Istituto Superiore per la Ricerca Ambientale (ISPRA), it was possible to install the first IDSL device in the same location where another sea level measurement, installed by ISPRA, is located. The installation location is inside a restricted military area, belonging to the local Coast Guard, thus very well secured (Fig. 3, 4).

The installation has been performed in November 2014; for the first two months very unstable behavior was present due to a bad choice of the solar panel voltage regulator. When the voltage (due to bad insulation and lack of battery power) was decreasing, the regulator did not switch off the load at 11V as expected but down to 4-5 V. This caused a block of the Raspberry that could not switch on again when the power was restored. As a consequence several missions to the site were necessary to recharge the battery and switch on back the device. After having changed the regulator in January 2015, the device worked fine without any major problem charging over the day and discharging over-night. Only in two occasions, in case of prolonged bad weather conditions, after 3.5 days of no sun, the device was off for few hours but when light returned, it switched back on as expected.

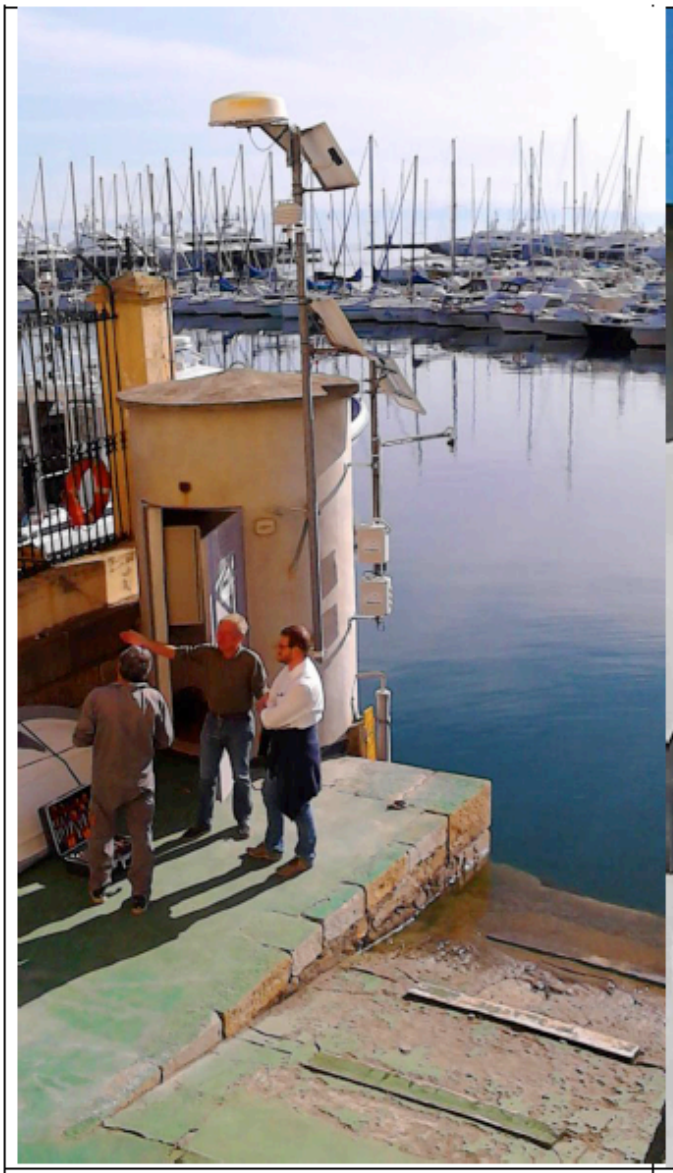

Figure 3 - The installation location in Imperia, inside the Porto Maurizio harbor

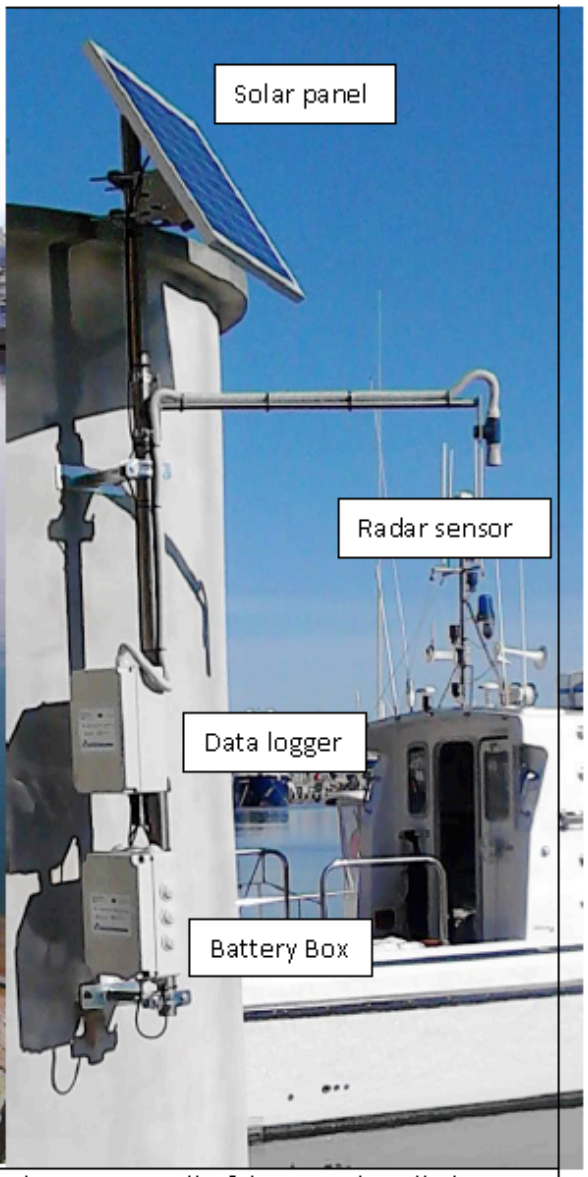

Figure 4 - Detail of the IDSL installation

Two major findings from the Imperia campaign are emerging:
- the large oscillations of the harbor sea level
- the important effect of the temperature on the sensor

The comparison of the sea level measured by the ISPRA mareograph and the IDSL showed that the IDSL was presenting quite extensive oscillations of several tents of cm that are not present in the ISPRA device (Figures 5 & 6). The ISPRA device is a wire ultrasonic sensor located inside a dumping pipe. In order to understand if this oscillation was real or not we have performed two pictures close to the measurement point, showing the position of the water surface. The pictures, in Figure 6, taken in a moment of high peak and low peak, show that indeed the oscillation is present and that the measurement was correctly reporting the 15 min period oscillation.

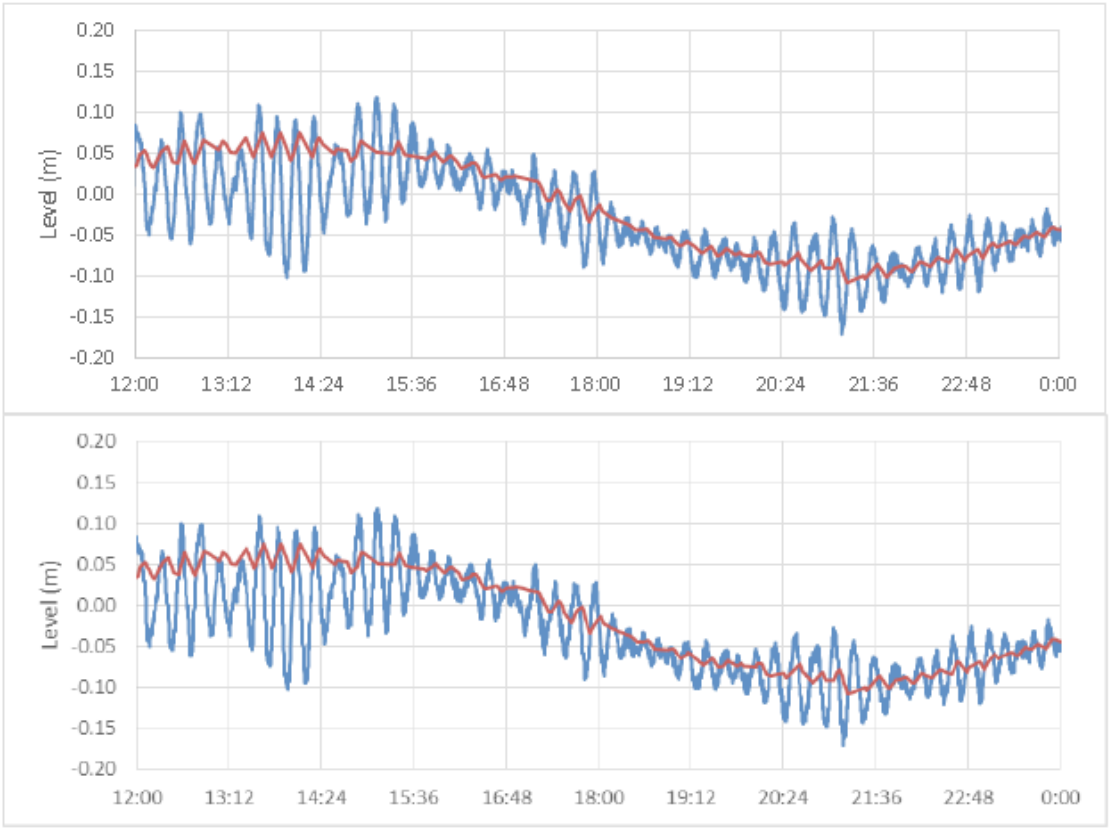

Figure 5, Measure sea level by the ISPRA tide gauge (red curve) and by the IDSL (blue curve)

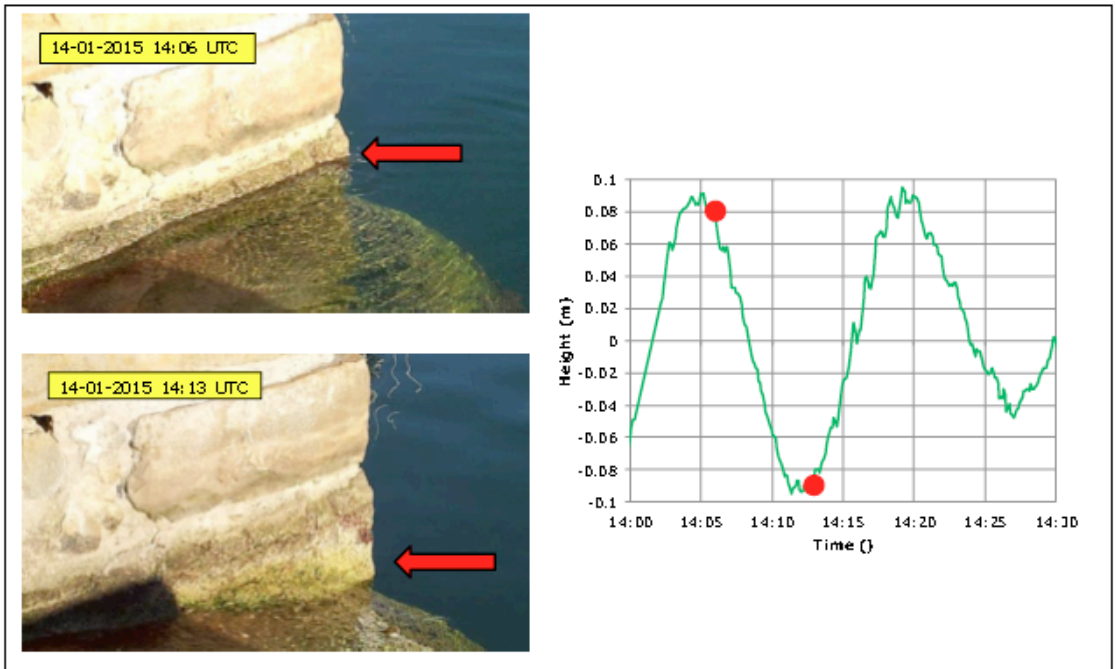

Figure 6 – Detail of the harbor oscillations on January 14th 2015

Two major findings from the Imperia campaign are emerging:

- the large oscillations of the harbor sea level
- the important effect of the temperature on the sensor

The comparison of the sea level measured by the ISPRA mareograph and the IDSL showed that the IDSL was presenting quite extensive oscillations of several tents of cm that are not present in the ISPRA device. The ISPRA device is a wire ultrasonic sensor located inside a dumping pipe. In order to understand if this oscillation was real or not we have performed two pictures close to the measurement point, showing the position of the water surface. The pictures, Figure 6, taken in a moment of high peak and low peak, show that indeed the oscillation is present and that the measurement was correctly reporting the 15 min period oscillation.

It would be interesting to perform an analysis of the harbor response to external sea level variations because if this is the case it could be that, in case of important events (i.e. Tsunami) this natural harbor oscillation could eventually lead to a large amplification factor, like in some locations in the Pacific (i.e. Crescent City or Hilo).

The temperature effect is still under checking (Fig. 7). The radar sensor is equipped with internal temperature compensation. This is necessary in order to have a signal that is as much as possible temperature independent and compensate the variation of the air sound speed as a function of temperature. The speed of sound in air increases by about 0.6 meters per second, per degree centigrade; this means that an increase of the air temperature of 1 degree centigrade, if not compensated, would result in a faster travel time and thus in a shorter time of fly below the sensor; the sensor would "believe" that the sea level is higher than in reality. Similarly an increase of the sensor temperature, not reflected in a similar increase of the air temperature could result in an over compensation and thus the sea level indicated would be lower. The actual air temperature of the path between the sensor and the target may not match the temperature measured at the sensor itself.

This is in fact what happens to the sensor installed in Imperia when there is hot sun shining: a progressive decrease of the indicated sea level in comparison with the reference sea level. As the sun decreases, or during cloud-cover days (we know it from the battery voltage behavior), the measured signal by both instruments is very similar.

In order to have the possibility to correct the discrepancy present in the sea level, we have found that the error shift in the sea level correlates well with the Raspberry CPU temperature (curve red in the upper plot of Figure 7). When the temperature increases above 40-41 degrees Celsius the shift appears. Although the use of the CPU temperature is an indirect estimation of the air temperature, this was the only available that we could use in the prototype device installed in Imperia. In the final device, we have included two air temperature sensors, one connected with the sea level device for a temperature compensation and another one to have the measurement transmitted to the server and eventually allow more direct correction, if necessary.

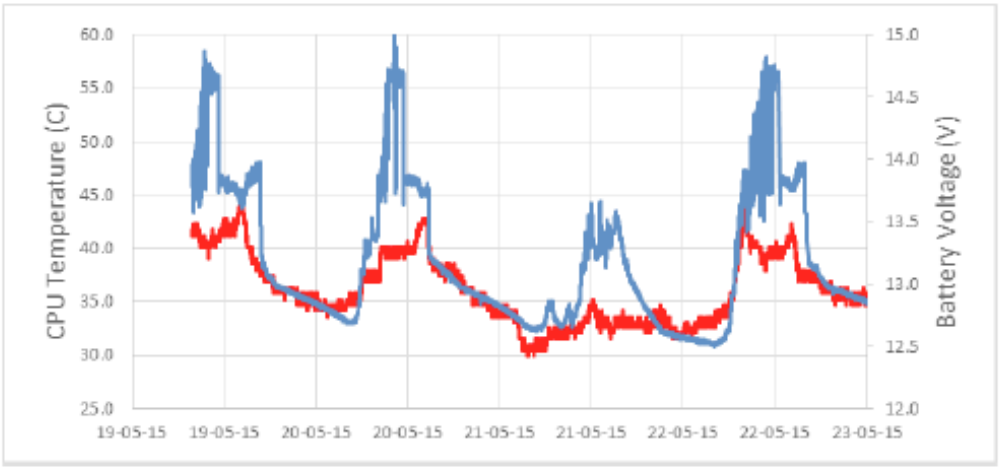

The left figure shows the classical battery charge/discharge cycle (blue curve): two days with very good solar insulation, the third day bad insulation and the fourth one with again good insulation. The red curve represents the CPU temperature of the Raspberry Pi+

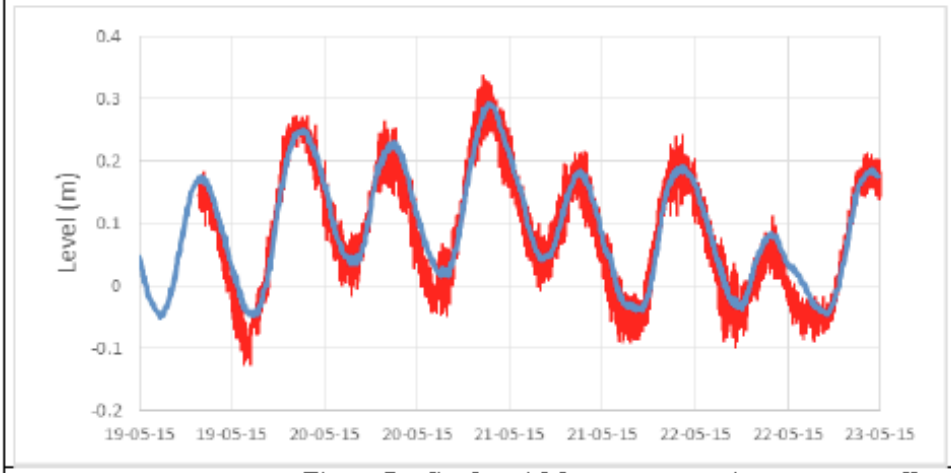

The comparison of the IDSL measured sea level (red) with the ISPRA sensor shows that in some periods, when the solar panel is charging, the IDSL deviates from the trend of the ISPRA signal, with a reduced value up to 6-7 cm in defect

Figure 7 – Sea Level Measurement and temperature effects

4. OFFER OF 20 IDSL TO UNESCO NEAMTWS

The Intergovernmental Coordination Group for the Tsunami Early Warning and Mitigation System in the North-eastern Atlantic, the Mediterranean and connected seas (ICG/NEAMTWS) was formed in response to the tragic tsunami on 26 December 2004, in which over 250,000 lives were lost around the Indian Ocean region. The Intergovernmental Oceanographic Commission of UNESCO (IOC-UNESCO) received a mandate from the international community to coordinate the establishment of the Tsunami Warning System.

One of the most important activities of the Warning Centers is · Collection, record, processing and analysis of sea level data for confirming and monitoring the tsunami or for cancelling elements of the alert system

Given the lack of instrumentation is some parts of the Mediterranean Sea this activity in some cases is not easy. For this reason the European Commission decided to support the development of

the system by offering the installation of 20 devices to the countries that are part of the NEAMTWS. After an international call of interest the following devices allocation has been attributed.

	Priority	Country	Organization	Status	Location	Zone	Survey
IDSL-01	0	Italy	JRC/IPSRA	Installed	Imperia	Tirrenian Sea	n.a.
1	1	Greece	NOA		Western Corinth Gulf	Aegean Sea	
2	1	Italy	INGV		Crotone	Ionian Sea	
3	1	Lebanon	CNRS	Surveyed	Batroun	Mediterranean East	3 Jun 2015
4	1	Maroc	CNRST		Casablanca	North Atlantic	
5	1	Portugal	IPMA	Surveyed	Sagres	North Atlantic	24 Apr 2015
6	1	Romania	NIEP	Surveyed	Mangalia	BlackSea	27-28 May 2015
7	1	Spain	IGN	Surveyed	Cadiz	North Atlantic	3-4 Jun 2015
8	1	Tunisia	INM		Tabarka	Mediterranean Central	
9	1	Turkey	KOERI	Surveyed	Fethiye	Mediterranean East	12 Jun 2015
10	2	Italy	INGV	Surveyed	Pantelleria	Mediterranean Central	15 Jun 2015
11	2	Maroc	CNRST		Marina Sidi Alabed (Rabat)	North Atlantic	
12	2	Portugal	IPMA	Surveyed	Albufeira	North Atlantic	24 Apr 2015
13	2	Romania	NIEP	Surveyed	Costanta	BlackSea	27-28 May 2015
14	2	Spain	IGN	Surveyed	Cartagena	Mediterranean West	3-4 Jun 2015
15	2	Tunisia	INM		Zarzis	Mediterranean Central	
16	2	Turkey	KOERI		Cesme	Mediterranean East	
17	3	Italy	INGV		Otranto	Ionian Sea	
18	3	Romania	NIEP	Surveyed	Sulina	BlackSea	27-28 May 2015
19	3	Turkey	KOERI		Kemer	Mediterranean East	
20	4	Turkey	KOERI		Foca	Mediterranean East	

As of June 2015, a number of surveys at the proposed installation sites has been performed and the precise locations and installation modes have been defined. Other surveys will be performed soon and the installation should be concluded before the end of 2015.

After the installation all the data will be available at the following JRC web site with the possibility to visualize or download the data for analysis purpose: http://webcritech.jrc.ec.europa.eu/tad_server

Figure 8 – Geographical distribution of the IDSL devices installation sites; the sites for Tunisia are not indicated as not yet available

5. CONCLUSIONS

The Joint Research Centre of the European Commission has developed a new mareograph for Tsunami and Storm Surge monitoring. The device is characterized by very high temporal (5 s) and space resolution (error<0.5 cm) connected with a low construction cost which makes possible a wide distribution of these devices to cover many areas in the Mediterranean Sea that lack of reliable and effective real time sea level measurements.

The initial experimental campaign organized by JRC in collaboration with ISPRA, showed very positive outcome for the first 6 months of continuous operation. This convinced the UNESCO/IOC to accept the proposal of JRC to test 20 new devices for an extended experimental campaign of at least 1 year. The new devices will be installed during 2015 and will be an important contribution to the development of the UNESCO Tsunami Early Warning System that is being built in the Mediterranean Sea and connected seas (Marmara and Black Sea) and North Atlantic areas.

AWCKNOWLEGMENTS

The JRC would like to acknowledge the Istituto Superiore per la Ricerca Ambientale (ISPRA) that allowed to conduct the Imperia experimental campaign; at the same time the Italian Coast Guard whose locations has been used for the physical installation.

REFERENCES

Annunziato, A. (2005). Development and Implementation of a Tsunami Wave Propagation Model at JRC. **Proceedings of the International Symposium on Ocean Wave Measurement and Analysis**. Fifth International Symposium on Ocean Wave Measurement and Analysis.

Annunziato, A. (2007). The Tsunami Assessment Modelling System by the Joint Research Centre. *Science of Tsunami Hazards* **26:2**, 70-92.

De Groeve, T.: Global Disaster Alert and Coordination System: More Effective and Efficient Humanitarian Response, **Proceedings of the 14th TIEMS Annual Conference**, 324-334, Trogir, Croatia, 2007.

ISSN 8755-6839

SCIENCE OF TSUNAMI HAZARDS

Journal of Tsunami Society International

Volume 34 Number 4 2015

COMPARATIVE NUMERICAL SIMULATION OF THE TOHOKU 2011 TSUNAMI

Baranova N.A.[1], Kurkin A.A.[1], Mazova R.Kh.[1], Pararas-Carayannis, G.[2]

[1]R.E.Alekseev Nizhny Novgorod State Technical University, Nizhny Novgorod, Russia
[2]Tsunami Society International, Honolulu, Hawaii, USA

ABSTRACT

The comparative numerical simulation of generation and propagation of tsunami waves generated by the source of the catastrophic 2011 Tohoku earthquake in Japan was performed based on the Okada model and the dynamic keyboard block model. The initial model is connected with the choice of orientation of longitudinal and transverse ruptures within the source region and the values of displacements along the main fault. A subsequent model is based on the premise that the initial stress distribution along the fault zone affects essentially the character of movements around the earthquake source and takes into account the stress-strain state of keyboard blocks. In the first case of the present study, the earthquake source was designated and constructed based on the parameters of the ten largest aftershocks within a finite time interval, while in the second case the source used included all aftershocks on the first day following the main event. Based on such comparative source simulations and far-field tsunami wave measurements, the results with both models were determined to have close similarities. However, in the near-field zone, the agreement with observable data was not as good. That can be attributed to inaccuracies in the placement of virtual tide gauges relative to real ones, as well as to features of bottom relief near the coast.

Keywords: *earthquake and tsunami of 2011 Tohoku, earthquake sources, tsunami source, tsunami modeling.*

Vol. 34, No. 4, page 212 (2015)

1. INTRODUCTION

On 11 March 2011, a great earthquake with Moment Magnitude of Mw = 9 occurred along the northeast offshore area of Honshu Island, in Japan. As noted in the scientific literature, this earthquake was much stronger than what had been expected. The sudden shift of the sea floor and the overall displacements generated tremendous tsunami waves, which, within minutes, struck the coasts of Honshu and Hokkaido Islands. The catastrophic waves ranged from 3 to 15 meters in height, destroyed many coastal cities and villages, killed more than 28,000 people and left about 500,000 more homeless. In certain areas and coastal valleys the waves inundated to a distance of up to 10 km inland (see, e.g. (10, 11, 21, 22, Lay and Kanamori 2011), causing colossal material damage. The waves destroyed the water-cooling units of the Fukushima-Daichi nuclear power plant, which led to a catastrophic eruption of radiation (10,11,21, Saito et al. 2011; Pararas-Carayannis 2014). There were power outages for about 4 million homes in Tokyo and the surrounding areas. The disaster left about 4.4 million homes in northeastern Japan without electricity and 1.4 million without water. Early estimates indicated that the monetary losses would far exceed $100 billion (Pararas-Carayannis 2014).

Comparing the Tohoku 11 March 2011 earthquake with predecessor events near the Sanriku coast, it can be determined that it was a typical example of a complex event including in all features of different types of catastrophic earthquakes (Fujii 2011). The process of propagation of the rupture in the source of this event occurred with a cascading failure mechanism, which was difficult to predict, and such a scenario of earthquake was not anticipated in any model of estimating seismic danger (Fujii 2011). A review of the combined rupturing impact on both the subducting Pacific oceanic lithosphere and on the overriding Eurasian tectonic plate (Pararas-Carayannis 2014), confirmed large vertical and horizontal tectonic crustal displacements by the quake's slow and long rupturing process, the three-dimensional dynamics of shallow and deeper subduction processes - as indicated by a spatial and a time sequence distribution and clustering of aftershocks - as well as effects of co-seismic lateral movements which compressed and deformed the sediments along the accretionary prism of the overriding plane near the Japan Trench.

1.1 Earthquake source of the Tohoku 11 March 2011 event.

The epicenter of main shock was located at 38.10° N, 142.86° E. The quake had a focal depth H=24 km, and a moment magnitude M_w=9.0 (21). It occurred about 373 kilometers (231 miles) away from Tokyo, about 130 kms (81 mi) off the east coast of Oshika Peninsula and about 150 km west of the tectonic boundary of the Eurasian and Pacific plates, characterized by the Japan Trench. Strong ground motions were felt as far away as Tokyo (Pararas-Carayannis 2014).

The extent of the source of aftershock distribution during the first day had dimensions of about 300x500 km, covering an area nearly 150,000 km². As described in a number of investigations (see, e.g. (11, Fujii 2011, Koper et al. 2011, Kanamori, 2011, Pararas-Carayannis 2014), the rupture begun very slow at the depth in 23-24 km. Within 45 sec after the onset of the earthquake there was sudden destruction of the accretionary wedge on the upper edge near the plate boundary along the Japan Trench. The affected area had dimensions of about 250×80 km^2

and produced displacements of up to 60 m. The rupture on the wedge along the trench continued for over 135 seconds and terminated near 36.5° S and near 39.5° N (10,11,21,22, Saito et. al. 2011, Fujii 2011). Further examination of the aftershock distribution (Pararas-Carayannis 2014) indicated three major clusters and that the seismic energy of the 2011 earthquake was mainly released about 100 km off the coast of Miyagi and Fukushima Prefectures. Plotting the aftershock focal depths along eastern Honshu by the same study, indicated that there was a spectacular peak of aftershocks at a focal depth of about 24 km, the depth at which the rupture begun. The significance of this to tsunami generation was evaluated in terms of regional, spatial subduction, geometry, slip, crustal movements and sediment displacements. Buckling of the crust due to subduction friction probably activated many minor, normal faults, which also gave rise to subsequent aftershocks - even outside the tsunami generating region on the outer ridge of the subducting plate. Indeed the aftershock distribution was extensive, confirming that the tsunami source area was indeed about 300 km wide and 500 km long (Pararas-Carayannis 2014).

A number of other investigations (Fujii 2011, Koper et al. 2011, Hirose 2011, Ito et al. 2011) also confirmed considerable displacements within the source region. The eastern coast of Japan moved eastward for up to 5 meters and subsided nearly to 1 meter, while the sea floor uplifted on the average of 5 m over an area of about 15,000 km2 (fig.1).

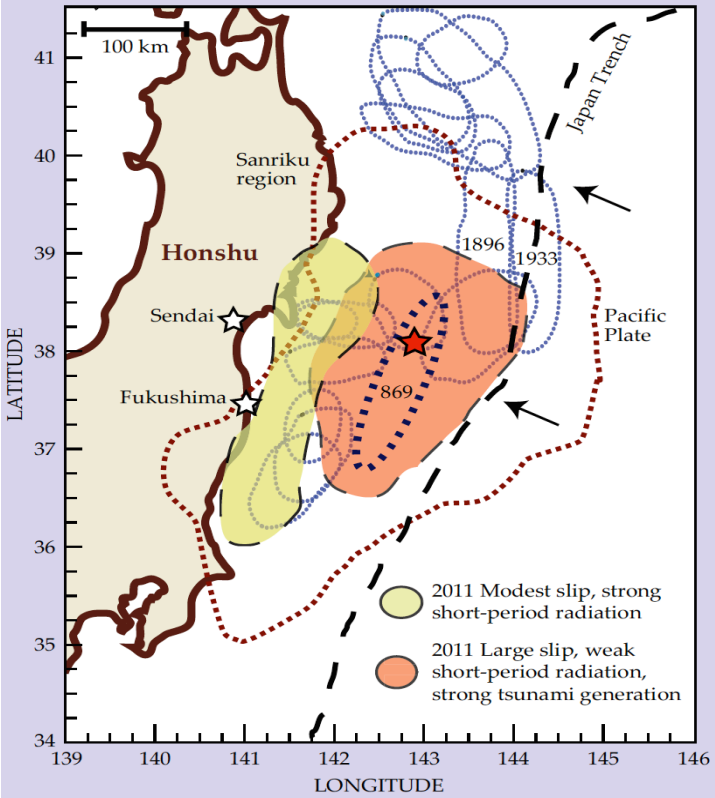

Figure 1. Seismic source of earthquake in Tohoku 11 March 2011 (Fujii 2011).

The direct measurements of sea bottom deformations had a maximum of 60-80 m along the outer portion of the accretionary ridge near the trench. Fig. 1 shows the approximate dimensions of the earthquake source (Fujii 2011) and the red asterisk the epicenter of the main shock of the 2011

earthquake and outlines the approximate area of subduction under the Island of Honshu (Hirose 2011). The black arrows indicate the direction of the Pacific plate motion relative to the Japanese volcanic arc. The area with the light-green color corresponds to the region of gradual shifts and the area with the dark-red color corresponds to the region of large displacement shifts, which generated the intensive tsunami waves. As stated previously the main displacements in the source region occurred during the first 150 sec after the main shock (Fujii 2011).

The grey dotted lines outline the region of the first-day aftershocks of the earthquake. Also shown in fig.1 is the region of historical earthquakes, which occurred in 1896 and 1933. The blue dashed curve shows regions of the strongest earthquakes, and the violet-colored points correspond to the assumed region of the strongest tsunami in the region, which occurred in the year 869 (Fujii 2011).

2. STATEMENT OF THE PROBLEM

Following the 2011 Tohoku-Oki earthquake, researchers from many countries performed numerical simulations of the tsunami event, using different approaches in generally stating the problem and in the numerical simulation itself (Kanamori 2011, Yomogida 2011, Baranova et.al. 2014, Hayashi 2011, Lovholt 2012, Imamura 2011,).

The structuring and initial configuration of the tsunami source area depends primarily on the character and the dynamics of crustal and sedimentary displacements within the earthquake source region. Presently, a number of mathematical models exist which numerically simulate a tsunami by taking into consideration the real geometry and the initial tectonic displacements of the seafloor (see, e.g. Kurkin 2004, Lobkovsky L.I., 2006). However, the determination of initial sea bottom displacements that contribute to tsunami generation is somewhat indefinite and depends on different possible scenarios. One of the present widely-used methods (see Okada 1985, Okada 1992, Imamura 2011) relates to the choice of orientation of longitudinal and transverse faults at the seismic source regions and on estimates of displacements along the rupture zone, which are difficult to evaluate and determine because of the extensive variability of such displacements for different events along and within different subduction zones. (Okada 1985, Okada 1992).

Based on earthquake magnitude alone, there are various correlation expressions being used to estimate the specific tsunami source characteristics. However, in order to determine the source parameters of tsunami generation, in addition to earthquake magnitude, it is essential to establish the vertical components of displacements of the sea floor and the orientation of the quake's rupture plane in the source region (Wells 1994). The displacement distribution on the sea floor for the case of a rectangular area of rupture is usually calculated with certain described formulas (Okada 1992). Furthermore, such studies use a solution of the static displacement of source segments in elastic semi-space, as calculated from crustal displacement distribution on its surface, which are then used to simulate a tsunami (Okada 1985, Okada 1992).

Another method in obtaining horizontal and vertical shifts within the tsunami source region has been presented in the literature (Lobkovsky 1988, Lobkovsky and Baranov 1984, Garagach and Lobkovsky 2006). It is well established that the strongest earthquakes near volcanic island arcs occur near the plane of contact between the base of the subducting plane and of the island arc

wedge and the most significant crustal displacements result of rupturing initiated along the plane of contact. As these studies demonstrate, the island arc wedge comprises separate large segments, which have been formed by transverse faulting. The presence of the faulting permits the introduction of new, smaller scale elements of interaction – keyboard blocks on the frontal edge of overriding plate (Lobkovsky 1988, Lobkovsky and Baranov 1984). Recent studies (Garagach and Lobkovsky 2006, Garagach and Ermakov 2001), are based on an elaborate geo-mechanical model in the subduction zone, based on the premise that the initial stress distribution affects essentially the crustal motion character near the earthquake source. Thus, taking into account the stress-strained state of keyboard blocks to obtain the dynamical components of vertical shift within the earthquake source area, a numerical simulation was performed on the processes within the seismic source (scenario 2), based on the program with the code name FLAC (dynamical keyboard model) (Lobkovsky 1988, Lobkovsky and Baranov 1984, Garagach and Lobkovsky 2006, Garagach and Ermakov 2001, Lobkovsky et al. 2006).

Using the two models in the present study, we performed a comparative numerical simulation of the tsunami generation source parameters and of the successive propagation of the tsunami in the Pacific Ocean basin.

3. SOURCE FORMATION OF THE TOHOKU 2011 TSUNAMI

3.1. Scenario 1

For a tsunami source for the first scenario, we used the seismic source described in the literature (Okada 1985, Okada 1992, Imamura 2011). This source was constructed on parameters of the ten strongest aftershocks, which occurred for some time interval (fig. 2).

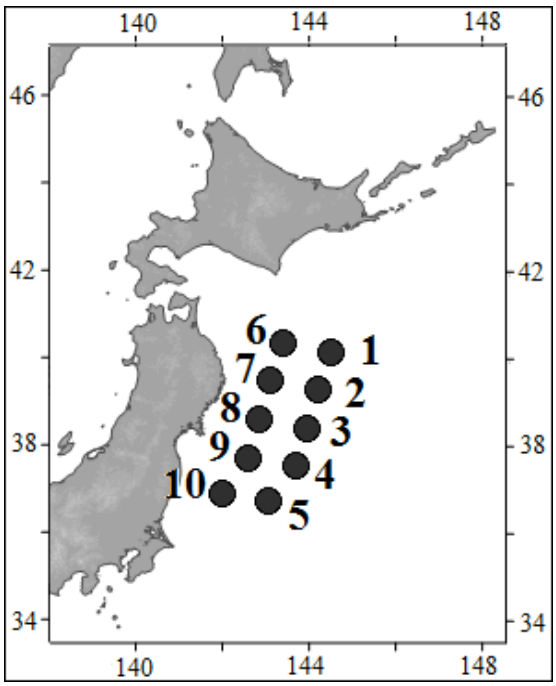

Figure 2. Aftershock locations of the earthquake of 11 March 2011 (Imamura 2011)

The distribution of vertical displacements on the sea bottom for a given source was calculated with formulas described by Okada (Okada, 1992). This source comprises of ten segments moving in different time intervals. The parameters that were used are the same for all the segments. Specifically, the length and width of the fault are the same (100 km). The fault rupture orientation (the strike angle) is 193°. The angle of plate inclination (the dip angle) is 14°, and the angle of plate displacement (slip angle) is 81°.

Based on the earthquake source parameters given in Table 1, one can obtain the heights of water level displacement at the source for each segment, using Okada's solution (Okada 1985, Okada 1992). Shown in columns 2-5 of Table 1, are the seismological and geodynamic data (Okada 1992, Imamura 2011), which was recalculated with the Okada formula. The last column shows the calculated initial displacement of water level at the tsunami source, as obtained with the same formula (Okada 1985, Okada 1992).

Table 1. The basic parameters of a seismic source (Kostenko et al. 2013).

Number of segment	Epicenter coordinates	Depth of source, km	Vertical displacement of source, m	Segment activation time, sec	Maximum displacement of water level, m
	1	2	3	4	5
1	40,168 N., 144,507 E.	1	20	0	12.49
2	39,300 N, 144,200 E.	1	10	0	6.24
3	38,424 N., 143,939 E.	1	35	30	21.87
4	37,547 N., 143,682 E.	1	15	30	9.37
5	36,730 N., 143,070 E.	1	2,5	60	1.56
6	40,367 N., 143,394 E.	24	1	60	0.5
7	39,496 N., 143,100 E.	24.2	3	90	1.5
8	38,620 N., 142,853 E.	24.2	4	90	1.99
9	37,744 N., 142,609 E.	24.2	2	120	0.99
10	36,926 N., 142,009 E.	24.2	2	120	0.99

The formation of the surface water wave for each segment (see Table 1) is presented in fig. 1. Immediately after the onset of the main event, segments 1 and 2 contribute to the initial sea level disturbance. After a time interval of about 30 sec, other source segments contribute to tsunami generation. The generation process is completed by the sea level displacements in segments 9 and 10. The process in whole occurs during a time interval of 120 seconds. As seen, all ten segments contribute to a bipolar type of displacement of wave level, which has a complex

form. The depression of sea level (blue color) faces the coasts of Honshu and Hokkaido islands, while the elevated sea level (yellow-red color), faces towards the open ocean.

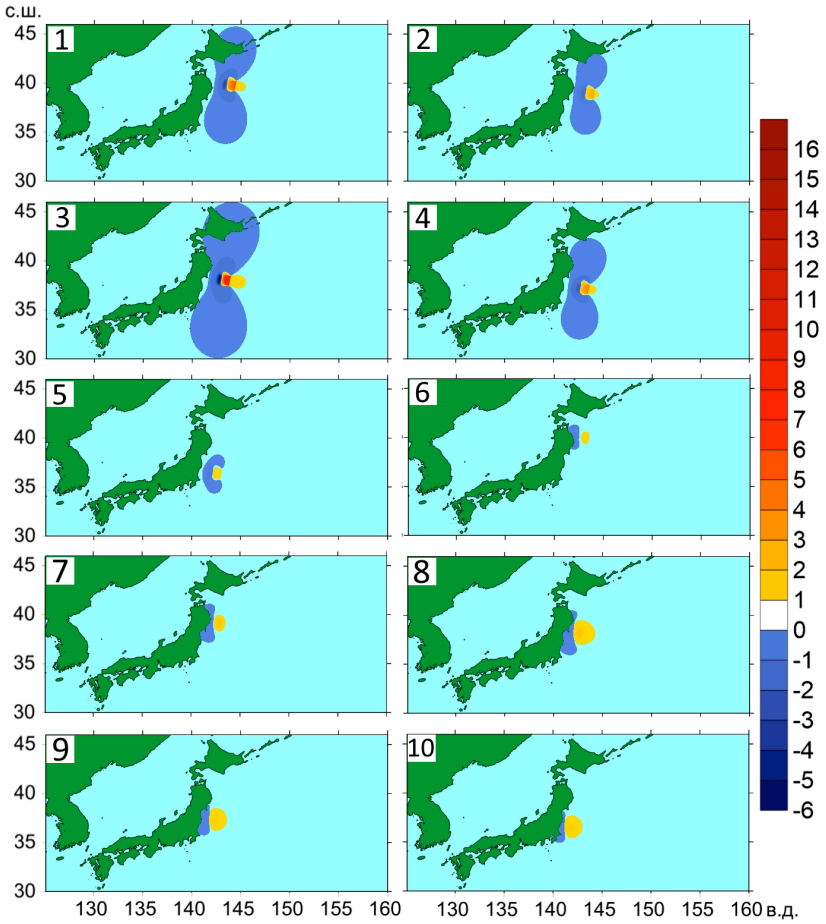

Figure 3. Formation of a tsunami source for scenario 1.

3.2. Scenario 2

The form of the seismic source for Scenario 2 was determined using data from NOAA's Center for Tsunami Research (http://nctr.pmel.noaa.gov/ honshu20110311/ namidance.ce.metu.edu.tr/; and from other researched (Lobkovsky and Baranov 1984, Baranova et al. 2014) (fig.4). For our numerical simulation processes of tsunami generation, the seismic source was that of Baranova et al. (2014) (see fig.4a).

To construct a geomechanical model of the subduction zone, a velocity cross-section was used as that described in recent work (Garagach and Ermakov 2001, Garagach and Lobkovsky 2006). Such a model takes into account both the density distribution and the distribution of tectonic stresses in the Earth's crust (Garagach and Ermakov 2001, Garagach and Lobkovsky 2006). Using data from other research work (22; Takahashi 2004), a numerical simulation of processes in seismic source was performed based on the program code FLAC (Baranova et al., 2014**,** Garagach and Lobkovsky, 2006)**.**

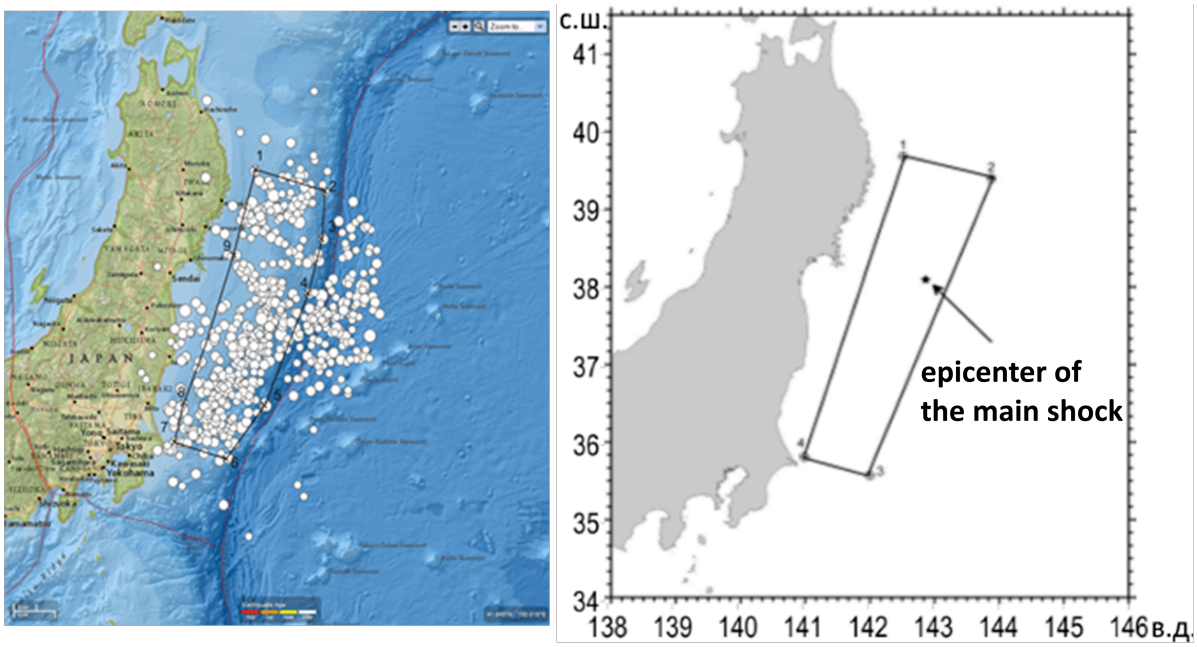

Fig. 4. a) Source of Tohoku earthquake of aftershocks of the first day. b) Simplified shape of earthquake source used under computation (Baranova et al. 2014).

The computational scheme in depicting the earthquake source zone is illustrated in Fig. 5. Apparently, and as also illustrated in Fig. 6, there was an accumulation of crust deformation intensity within the seismic source, which contributed to the distribution of vertical displacement during the pre-earthquake period (Baranova et al. 2014).

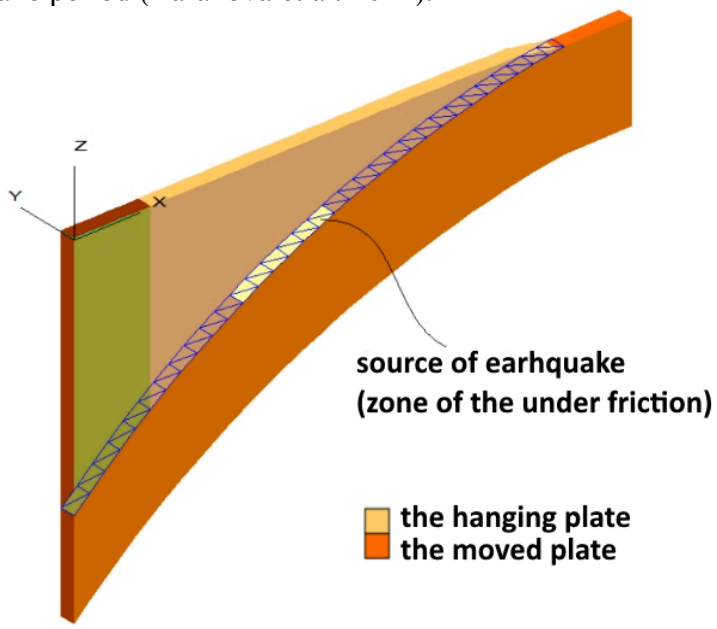

Figure 5. Calculated scheme of a zone of an earthquake source (Baranova et al. 2014, Garagach and Lobkovsky 2006).

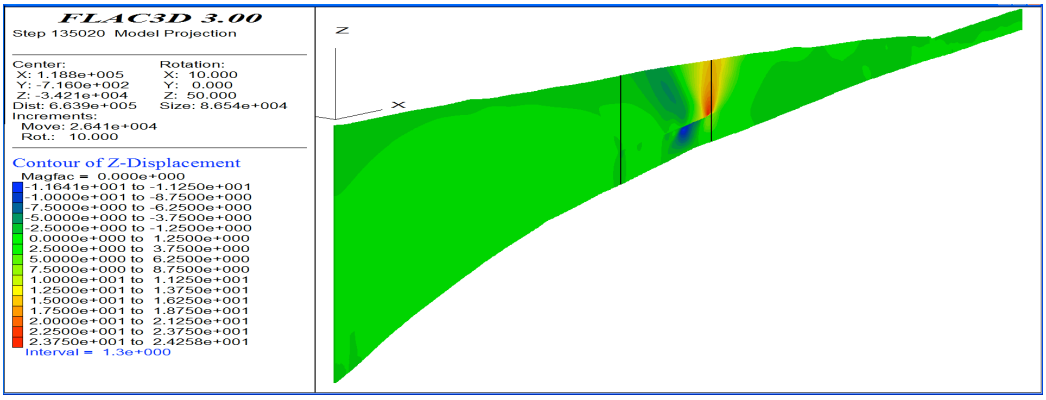

Figure 6. Vertical displacement after an earthquake. Vertical lines selected a section on which there was a reduction of friction coefficient (Baranova et al. 2014, Garagach and Lobkovsky 2006).

In our study, we examined the earthquake source as a motion of a single block which extended from 70 to 150 km (Fig. 5,6) on the X-axis - as delineated graphically in Fig. 7 - taking into account the intensity of the initial stress before the occurrence of the main earthquake (Garagach and Ermakov 2001, Garagach and Lobkovsky 2006), which Baranova et al. (2014), calculated within the frames of the program coded as FLAC. Illustrated by Fig. 7 are the changes of vertical displacement of the sea floor during the earthquake in the seismic source region from its beginning $t = 0$ for a time period $t = 135$ seconds.

The beginning of the earthquake process was very indistinct, particularly during the first five seconds. During the time interval of 30-45 seconds, the crustal expansion accelerated and the displacements amplified. After this time period, the rupture continued for another 45 seconds in a northern direction and terminated 135 seconds after the onset of the main earthquake. (Fujii 2011, Koper et al. 2011, Kanamori 2011).

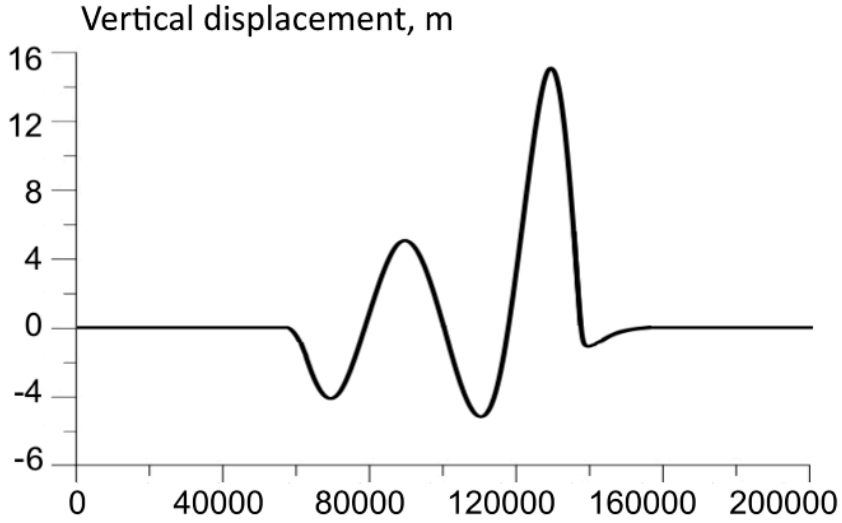

Figure 7. Plots of change of vertical displacements (Baranova et al., 2014).

4. NUMERICAL MODELING

The analysis of the two scenarios was performed by numerical simulation using square block areas which extended from 120˚ E - 115˚ W, from 60˚ N – 60˚ S, from 120˚ E - 160˚ E, and from 30˚ N – 46˚, along the eastern Pacific coast of Honshu Island. One of the computation basins is presented in Fig. 8. The bathymetry of this region was taken from the GEBCO Digital Atlas, which has a 30-arcsec resolution [5]. The grid step for the analysis averaged about 900 meters.

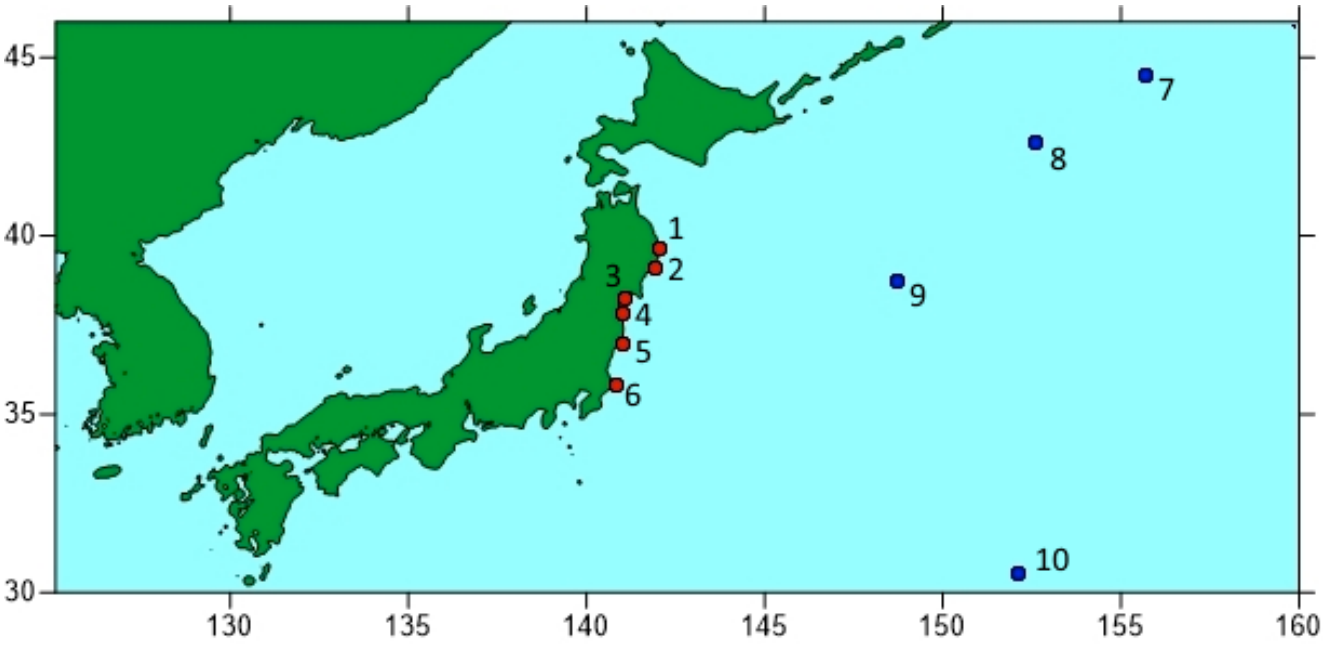

Figure 8. The computational area. The red points 1-6 correspond to the assigned position of virtual tide gauges along the coastal zone; the blue points 7-10 correspond to position of the measuring DART instruments.

To compare the results of the numerical simulation and for comparison with the observational data, virtual tide-gauges were chosen along coastal location points of Honshu Island in Japan where the maximum measurements of sea levels had been observed (Fig. 9). However, some differences in the location of computational points and of the real tide gauges, connected with technical features of numerical simulation, can lead to some dispersion in the record of the height and period of sea level oscillations.

4.1. Scenario 1

The numerical simulation of Scenario 1 was realized by using the program complex NAMI DANCE [31], which solves the shallow water equations written in spherical coordinates and by taking into account the Earth's rotation (Coriolis Force):

$$\frac{\partial M}{\partial t}+\frac{1}{R\cos\theta}\frac{\partial}{\partial\lambda}\left(\frac{M^2}{D}\right)+\frac{1}{R\cos\theta}\frac{\partial}{d\theta}\left(\frac{MN\cos\theta}{D}\right)+\frac{gD}{R\cos\theta}\frac{\partial\eta}{\partial\lambda}+\frac{gn^2}{D^{7/3}}M\sqrt{M^2+N^2}=fN,$$
$$\frac{\partial N}{\partial t}+\frac{1}{R\cos\theta}\frac{\partial}{\partial\lambda}\left(\frac{MN}{D}\right)+\frac{1}{R\cos\theta}\frac{\partial}{d\theta}\left(\frac{N^2\cos\theta}{D}\right)+\frac{gD}{R}\frac{\partial\eta}{\partial\theta}+\frac{gn^2}{D^{7/3}}N\sqrt{M^2+N^2}=-fN, \quad (3)$$
$$\frac{\partial\eta}{\partial t}+\frac{1}{R\cos\theta}\left[\frac{\partial M}{\partial\lambda}+\frac{\partial}{\partial\theta}(N\cos\theta)\right]=0$$

where η is a sea level change, M and N are components of water discharge along latitude λ and longitude θ; D is the total depth of the basin; g is the gravity acceleration; R is the Earth's radius, f is the Coriolis parameter and n is the bottom friction coefficient. For the computation, the value n = 0.0015 $m^{-1/3}c$, is used which is characteristic for natural bottom (sand, pebbles). The equations are solved within the framework of the nonlinear dispersion theory of long waves, where physical dispersion is replaced by a numerical one (Kostenko et.al. 2013). Under the present simulation a time step in 1 sec was used, thus satisfying the Courant condition. At the open Pacific front, the boundary conditions are stated in the form of free wave passing.

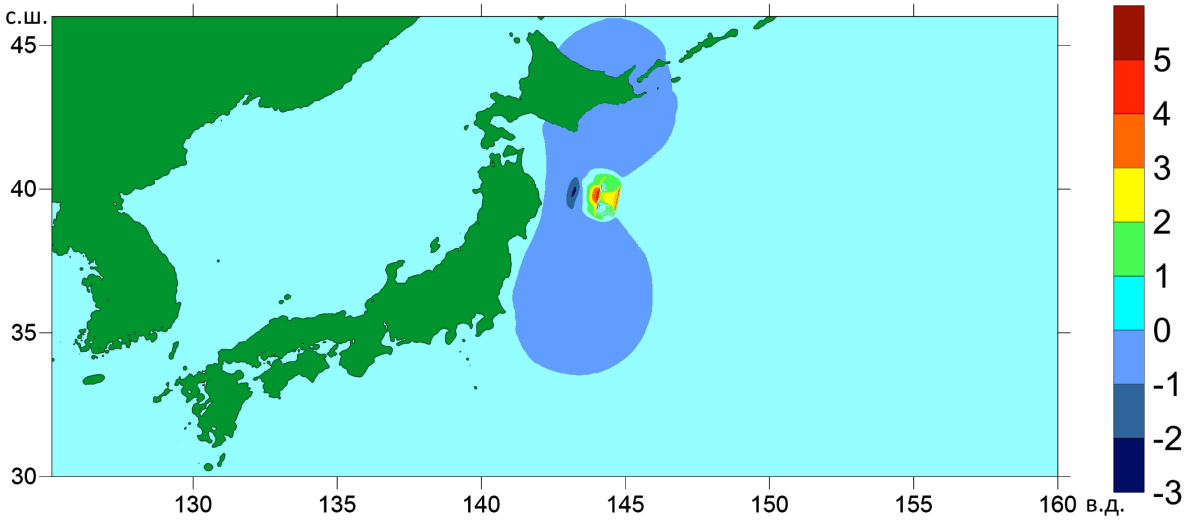

Figure 9. The tsunami source generated on 120 sec (Scenario 1).

Presented in fig. 9 is the areal configuration of the tsunami source, taking into consideration all of the 10 segments of block displacements – after an interval of 120 seconds from the onset of the main quake. Presented In fig.10 are the advancing tsunami wave fronts for six time moment intervals. As shown, practically at all coastal points of Honshu and Hokkaido islands, the tsunami is initiated with a withdrawal of seawater from the beaches. A clearer illustration of the distribution of maximum tsunami wave height on the basin is presented in fig. 11.

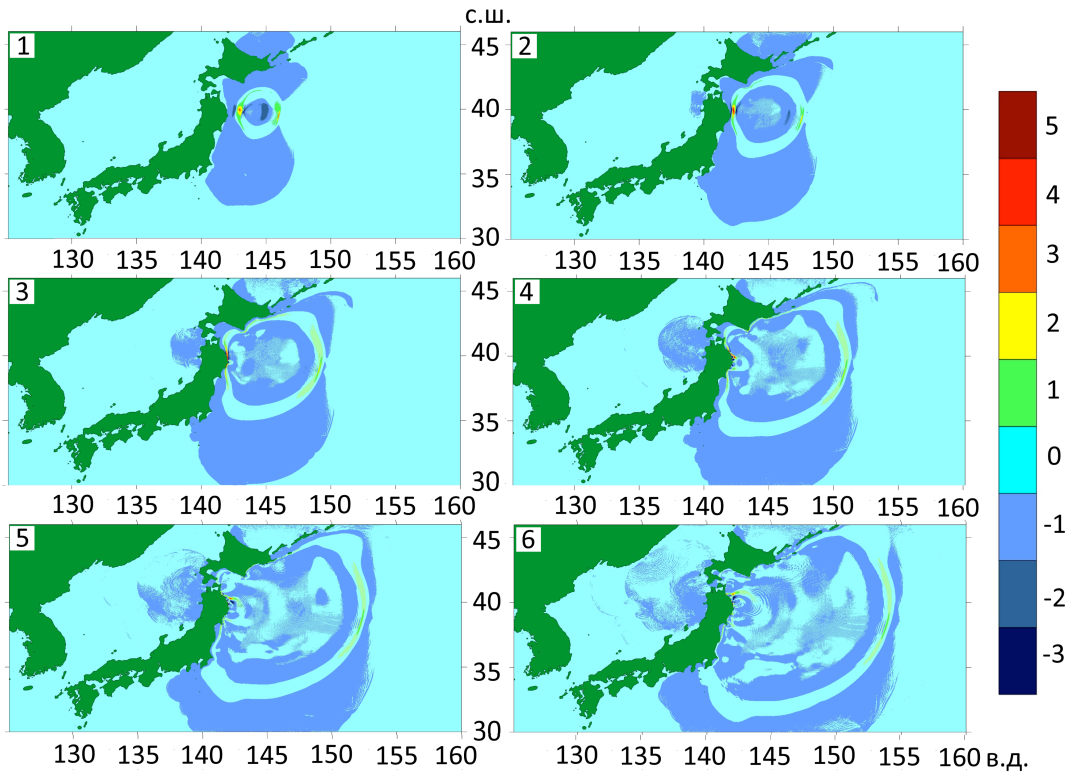

Figure 10. Position of wave fronts for 6 time moments ranging: 1 - 10 min, 2 - 20 min, 3 - 30 min, 4 - 40 min, 5 - 50 min, 6 - 60 min.

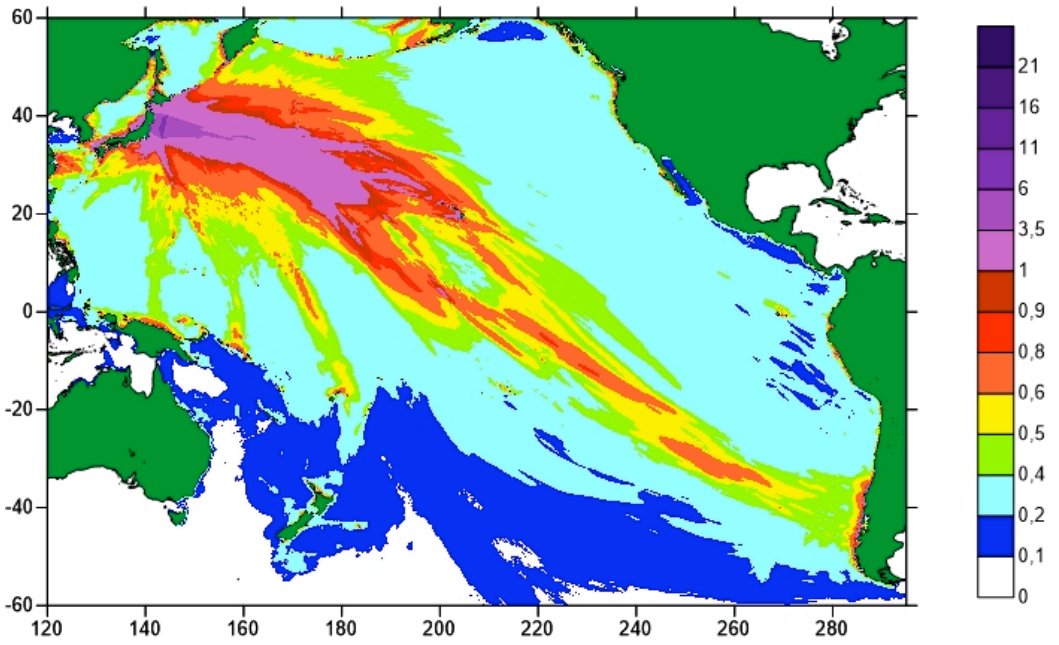

Figure 11. Maximum distribution of tsunami wave energy flux in the Pacific Ocean based on implementation of scenario 1.

4.2. Scenario 2

The tsunami source for Scenario 2 was determined by use of the dynamical keyboard model (Lobkovsky 1988, Garagach and Ermakov 2001, Garagach and Lobkovsky 2006, Lobkovsky, Mazova et al. 2006).

To describe the tsunami simulation from the earthquake source, a system of nonlinear shallow water equations was used as described in the scientific literature (Lobkovsky, Mazova et al. 2006). A system of nonlinear shallow-water equations (as in Lobkovsky at el. 2006) was used for the numerical simulation of tsunami generation from the 2011 Tohoku, Japan earthquake as follows:

$$\begin{cases} \dfrac{\partial u}{\partial t} + u\dfrac{\partial u}{\partial x} + v\dfrac{\partial u}{\partial y} + g\dfrac{\partial \eta}{\partial x} = f_1 \\ \dfrac{\partial v}{\partial t} + u\dfrac{\partial v}{\partial x} + v\dfrac{\partial v}{\partial y} + g\dfrac{\partial \eta}{\partial y} = f_2 \\ \dfrac{\partial \eta}{\partial t} + \dfrac{\partial}{\partial x}[(\eta + H - B)u] + \dfrac{\partial}{\partial y}[(\eta + H - B)v] = \dfrac{\partial B}{\partial t} \end{cases} \tag{6.1}$$

where $f_1 = \dfrac{-C_h}{H+\eta} u\sqrt{u^2+v^2}$, $f_2 = \dfrac{-C_h}{H+\eta} v\sqrt{u^2+v^2}$ are the bottom friction; *x,y* are the space coordinates along the axes *Ox* and *Oy,* respectively; *t* is the time; *u*(*x*, *y, t*), *v(x, y, t)* are the average over depth horizontal components of fluid flow rate; $\eta(x,y,t)$ is the displacement of free surface relatively its undisturbed level; *H* is the maximum depth of the basin at undisturbed water, function $B(x,y,t)$ describes displacement of bottom surface relatively initial position (accounting to dynamic characteristics of seismic motion); g is the gravity acceleration, $Ch = \dfrac{(H+\eta-B)^{0.4}}{sh}$ is the bottom friction coefficient (Shezi coefficient), and sh is the roughness coefficient.

Figure 12 depicts four time moments of the tsunami source generation of the Tohoku 2011 earthquake for Scenario 2 (see fig. 7). The two peaks of vertical change in this figure are shown in yellow and red colors (2 and 4 panels). To two minimums in the same figure 12 are shown in dark-blue and blue colors (1 and 3 panels). After the formation of the tsunami source, the wave begins to propagate towards both the coast of Honshu Island and the open ocean.

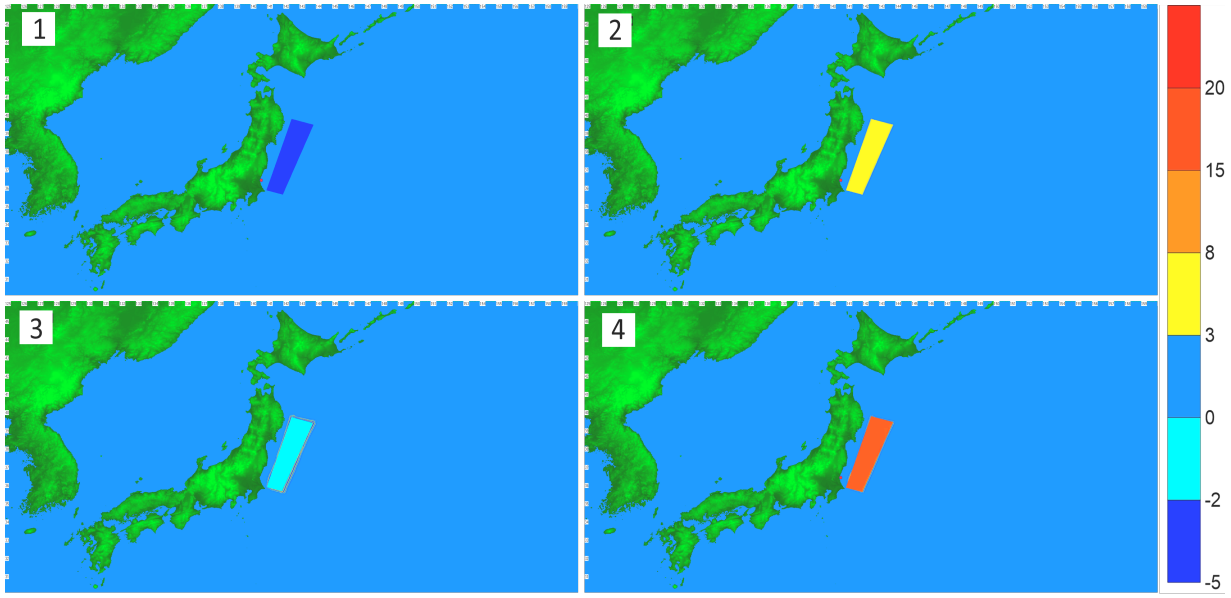

Fig.12. Generation of the dynamic source (scenario 2). 1. H= -4 m. 2. H = +5 m. 3. H = -5 m. 4. H = +15 m.

Fig.13 shows the propagation of the wave fronts for six time moments. It is well seen from the simulation that the initial tsunami wave at Honshu Island arrives in 15-20 min, and that the maximum tsunami wave height at Miyako is more than 20 meters. At Hokkaido island the tsunami wave arrives in 32 minutes and that a wave with a maximum height near 3.6m arrives at Erimo in 58 minutes.

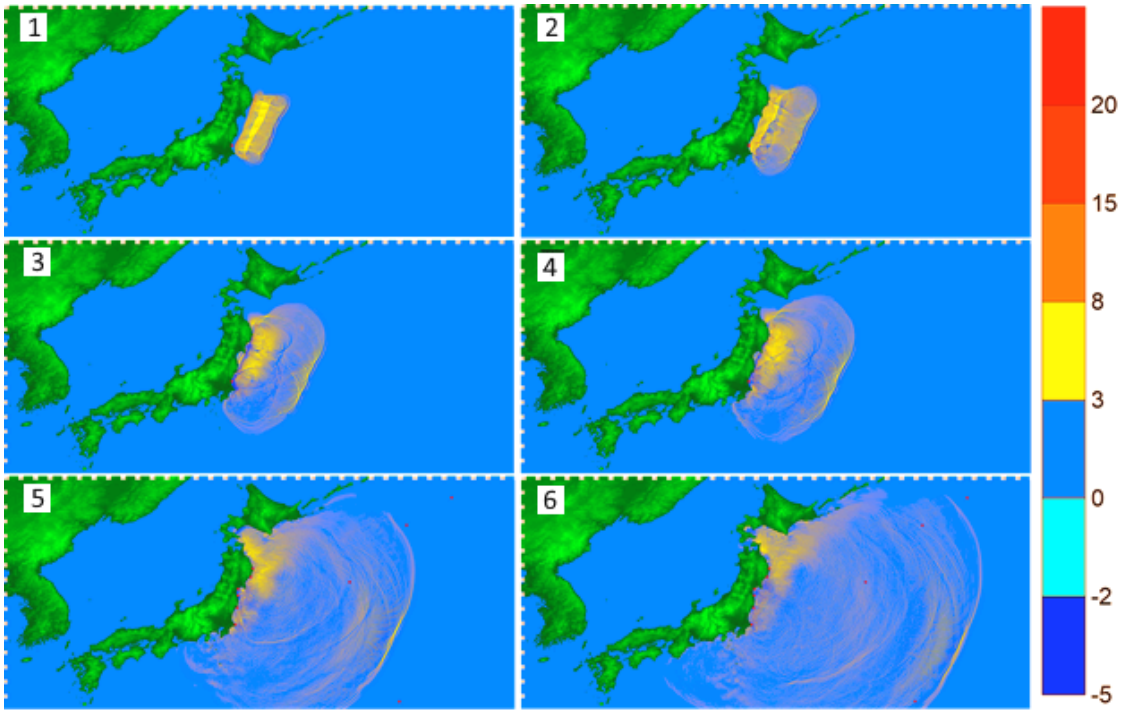

Fig.13. Position of wave fronts for time moments: 1 – 10 min,2 - 20 min, 3 – 25 min, 4 – 30 min, 5 – 45 min, 6 – 60 min. 2- 20 мin, 3 – 25 мin, 4 – 30 мin, 5 – 45 мin, 6 – 60 мin.

Fig.13 shows the distribution of computed maximum tsunami wave heights based on the implementation of scenario 2. As shown, the greater intensity of wave energy focuses on the central part of Honshu Island. Near Hokkaido Island and the Kurile islands, the wave heights are not larger than 7-8 meters.

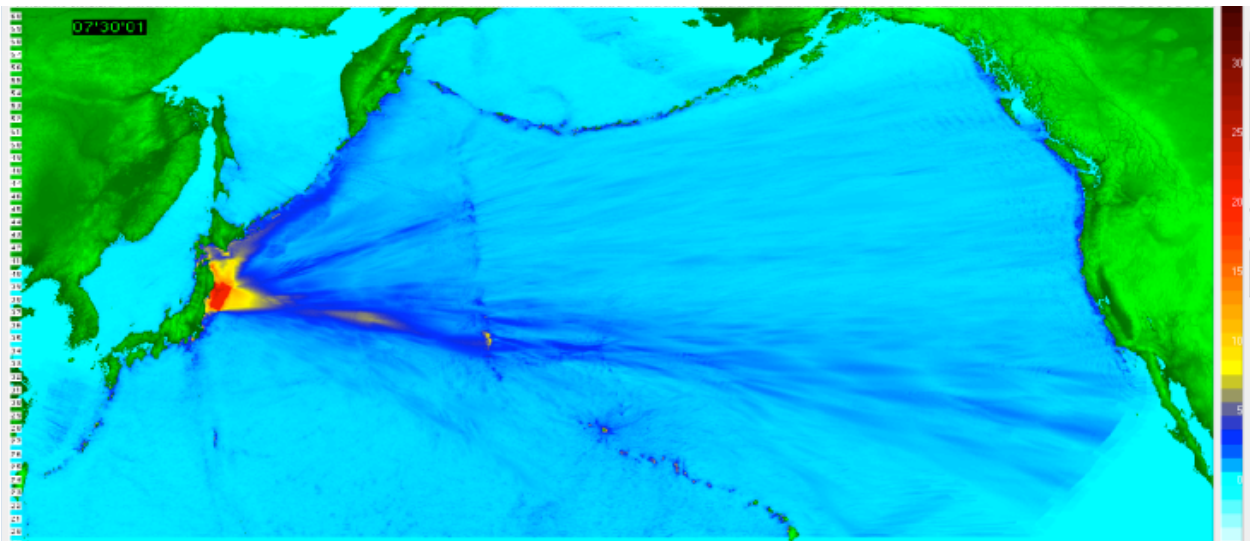

Fig.14. Maximum distribution of waves in the water area of the Pacific Ocean in case of implementation of the scenario 2.

4.3 Comparison of real data and results of calculations with the Okada model (Okado 1992) and the model of dynamic source (Baranova et al. 2014).

The results of computation for the first and second tsunami waves for the 2011 Tohoku Japan event that were performed with the Okada model as well as with the dynamic source are presented in Table 2. Shown in the first line of the column with the heading «Coordinate pp», are the coordinates of the of real event (from Saito et al. 2011) and in the second line the coordinates of the virtual tide gauges.

As seen from Table 2, for a number of coastal points as for example Miyako, for both first and second scenarios there is good agreement between the observed/recorded data from tide gauges and the results of the numerical simulation. Antithetically, from Sendai to Choshi the agreement between computed and observational data is noticeably poorer. At Ofunato, the computation with the model of dynamical source gives somewhat good agreement with the observational data, particularly for the second wave. However, at Goshi, although the tide gauge data shows the first wave to be a positive flooding wave followed by a negative wave of withdrawal, the computation data in both models gives a reciprocal picture, and at all computation points the tsunami begins with the withdrawal of water from a beach which is accompanied by second depression wave. Since such a picture is observed for both Scenario 1 and Scenario 2, which are independent from one other, such differences of the data can be associated with small-scale bottom relief features at this part of the shelf. At the deep-water DART tsunami recorders, the picture is essentially better

and the computed phase relations of the wave are consistent with the observational data. The first wave is a positive elevation wave, followed by a depression wave. For DART21-401 station the computed and observation data are in agreement for both models. For DART21-419 station, the results of computations with the dynamic model are in better agreement with the observational data while for station DART21-418 the agreement of computed and observation data is better with the Okada model. In the case of station DART21-413, the observation data is in good agreement only with computation of the second wave (depression wave) using the Okada model.

Table 2

N	Points	Coordinate pp. 1.Real data 2.Scenario 1 3.Scenario 2	Real data		Scenario 1		Scenario 2	
			1		2		3	
			First wave	Second wave	First wave	Second wave	First wave	Second wave
1	Miyako	141.9830 39.6500 142.0662 39.6433	-1.2	+7.7	-2.7	+6.8	-1.1	+7.8
2	Ofunato	141.7500 39.0170 141.9161 39.0594	-2	+7	-1.3	+2.7	-1.2	+7
3	Sendai	141.0330 38.2670 141.0653 38.2252	-1.3	+5	-0.3	+1.6	-0.8	+3.3
4	Soma	140.9500 37.8170 141.0486 37.7914	-1.8	+8.7	-0.19	+1.7	-1.4	+5.7
5	Onahama	140.8833 36.9369 140.9985 36.9405	-0.7	+2	-0.1	+0.6	-1.1	+4.2
6	Choshi	140.8670 35.7500 140.8651 35.7893	+2	-1	-0.1	+0.7	-0.7	+2.5
7	DART21 419	155.7000 44.5000 155.6959 44.5151	+0.7	-0.2	+0.35	-0.63	+0.75	-0.3
8	DART21 401	152.6000 42.6000 152.6096 42.6131	+0.8	-0.2	+0.9	-0.6	+0.5	-0.3
9	DART21 418	148.7000 38.7000 148.7059 38.7090	+2	-1	+1.87	-0.88	+1,.2	-0.5
10	DART21 413	152.1000 30.5000 152.1091 30.5005	+0.7	-0.2	+0.3	-0.24	+0.4	-0.3

5. CONCLUSIONS

Since in the near-field zone the tsunami generation mechanisms are affected by both the configuration and the dynamics of the seismic source, there is an obvious difference between the values of tsunami wave height obtained with both Scenarios 1 and 2 of the present study. On the other hand, at a distance of more than three tsunami wavelengths, both the shape and the influence of the seismic source area become less essential. This is probably the reason that more consistent values are obtained for deep-water DART tsunami stations for both Scenarios 1 and 2. As for the comparison with values of wave heights from real tide gauges, an essential factor of differences are their location as compared with the chosen locations of virtual tide gauge stations - since in the coastal zone there are essential effects of amplification due to convergence of the waves, in

addition to subsequent reflections. So, for rough estimates of numerical simulation of tsunami generation and propagation of waves using both for Models 1 and 2, it can be concluded that for near-field sources (for coasts of Honshu and Hokkaido islands) most coastal points do not demonstrate a good agreement with the data obtained from tide gauges and that can be attributed to both coastal configuration and features of the local submarine relief. However, for far-field regions the values of maximal wave height are in better agreement. Finally, it should be emphasized that an important factor is also the initial crustal stress distribution before the earthquake's onset.

ACKNOWLEDGEMENTS

The presented results were obtained within the framework of the state order in the sphere of scientific activity (Tasks № 2015/133 ("organization of scientific research" and project No. 2839).

REFERENCES

1. Baranova N., Baranov B., Lobkovsky L., Mazova R., 2014. New approach to the analysis of strongest earthquake Tohoku 2011: Int. Workshop on Mega Earthquakes and Tsunamis in Subduction Zones: Forecasting Approaches and Implications for Hazard Assesment (Rhodes Isl., Greece, 6-8 October, 2014), Abstr. Book, p.23-24.
2. Fujii Y., 2011. Tsunami source of the 2011 off the Pacific coast of Tohoku Earthquake: Earth Planets Space Letters, 63, pp.815–820.
3. Garagash I.A., Lobkovsky L.I., 2006. An analysis of the dynamic displacement process of the sea bottom due to a subduction zone earthquake: 4th International FLAC Symposium on Numerical Modeling in Geomechanics – 2006. Symp.Proc. (Hart & Varona (eds.)) pp.06-01.
4. Garagash I.A., Ermakov V.A., 2001. Using of geology-geophysical models for modeling of stressed state of Earth crust on example of Sakhalin island and North Tyan-Shan: III Scientific Conference "Problems of seismicity of Far East", Khabarovsk, Russia, 2001. Conf. Proc. pp.23-27.
5. GEBCO world map. URL: http://www.gebco.net/data_and_products/gebco_world_map/
6. Hayashi Y. et al., 2011. Tsunami source area of the 2011 off the Pacific coast of Tohoku Earthquake determined from tsunami arrival times at offshore observation stations: Earth Planets Space Letters, 63, pp.809–813.
7. Hirose F., Miyaoka K., Hayashimoto N., Yamazaki T., Nakamura M., 2011. Outline of the 2011 off the Pacific coast of Tohoku Earthquake (M_w 9.0): Seismicity: foreshocks, mainshock, aftershocks, and induced activity: Earth Planets Space. 63. pp. 513–518.
8. Ito Y., Tsuji T., Osada Y.,. Kido M, Inazu D., Hayashi Y. et al., 2011. Frontal wedge deformation near the source region of the 2011 Tohoku-Oki earthquake: Geophys. Res. Lett. 38, p. L00G05, DOI:10.1029/2011GL048355.
9. Imamura F., 2011. Tohoku University Source Model version 1.0 of Great East Japan Tsunami. (Due on June 06, 2011).

10. JAMSTEC.URL:http://www.jamstec.go.jp/j/about/pressrelease/20110428/
11. Japan Meteorological Agency. URL: http://www.jma.go.jp/jma/ indexe.html
12. Koper K.D., Hutko A.R., Lay T., Ammon C.J., Kanamori H., 2011. Frequency-dependent rupture process of the 2011 M_w 9.0 Tohoku Earthquake: Comparison of short-period P wave back projection images and broadband seismic rupture models: Earth Planets Space. 63. pp. 599–602.
13. Kanamori H., Yomogida K. (Guest Eds.), 2011. First Results of the 2011 off the Pacific coast of Tohoky Earthquake / In: Earth Planets Space, Special Issue. 63.
14. Kurkin A.A., Pelinovsky E.N., Choi B.H., Li D.S., 2004. A comparative estimation of the tsunami hazard for the Russian coast of the Sea of Japan based on numerical simulation: Oceanology 44, pp.163-172.
15. 15.Kostenko I.S., Zaitsev A.I., Yalchenir A., Rybin A.V., Yarkin D.C., 2013. Manifestation of 2011'th Tohoku tsunami near Kuril islands and Sakhalin island: Transactions of NNSTU n.a. R.E. Alekseev. 2 (99), pp. 43-51.
16. Lay T., Kanamori H., 2011. Insights from the great 2011 Japan earthquake: Phys.Today 64, pp.33-39.
17. Lovholt F. et al., 2012. Modeling propagation and inundation of the 11 March 2011 Tohoku tsunami: Nat. Haz. Earth Syst. Sci., 12, pp.1017–28.
18. Lobkovsky L.I., 1988. Geodynamics of spreading and subduction zones and two-level plate tectonics(Nauka Press, Moscow, USSR, 1988).
19. Lobkovsky L.I., Baranov B.V., 1984. Keyboard model of strong earthquakes in island arc and active continental edges: Doklady, 275, pp.843-847.
20. Lobkovsky L.I., Mazova R.Kh., Kataeva L.Yu., Baranov B.V., 2006. Generation and propagation of catastrophic tsunami in basin of Okhotsk Sea. Possible scenarios: Doklady, 410, pp.528-531.
21. Magnitude 8.9 – NEAR THE EAST COAST OF HONSHU, JAPAN 2011 March 11 05:46:23 UTC. URL: http://earthquake.usgs.gov/earthquakes/recenteqsww/Quakes/busc0001xgp.php .
22. NOAA Center for Tsunami Research – http://nctr.pmel.noaa.gov/ honshu20110311/ namidance.ce.metu.edu.tr/
23. Mori, N., and Takahashi T. 2012. The 2011 Tohoku Earthquake Tsunami Joint Survey Group, 2012. The 2011 Tohoku Earthquake Tsunami Joint Survey Group (2012), Nationwide Post Event Survey and Analysis of the 2011 Tohoku Earthquake Tsunami, Coastal Engineering Journal, Vol. 54, Issue 4, 1250001, 27 p, doi:10.1142/S0578563412500015
24. Okada Y., 1985. Surface deformation due to shear tensile faults in a half-space: Bull. of the Seismological Society of America, 75, pp.1135-1154.
25. Okada Y., 1992. Internal deformation due to shear and tensile faults in a half-space: Bull. Seismol. Soc. Am., 82, pp.1018–1040.
26. Pararas-Carayannis G., 2014. The Great Tohoku-Oki Earthquake and Tsunami of March 11, 2011, in Japan. Pure Appl. Geophys. 171, 3257-3278, Springer, DOI 10.1007/s00024-013-0677-7 Erratum on the distribution of inundation and wave heights along the coastline of Eastern Honshu as determined by the comprehensive survey summarized by Mori et al. (2011) and by Mori et al. (*2012*) or other investigations.

27. Saito T., Ito Y., Inazu D., and Hino R., 2011. Tsunami source of the 2011 Tohoku-Oki earthquake, Japan: inversion analysis based on dispersive tsunami simulations: Geophys. Res. Lett. 38.
28. Takahashi N. et al., 2004. Seismic structure and seismogenesis off Sanriku region, northeastern Japan: Geophys. J. Int. 159, pp.129-145.
29. Wells D.L., Coppersmith K.J., 1994. New empirical relationships among magnitude, rupture length, rupture width, rupture area, and surface displacement: Bull. Seism. Soc. Am. 84, pp. 974-1002.
30. Yomogida K, Yoshizawa K, Koyama J, and Tsuzuki M., 2011. Along-dip segmentation of the 2011 off the Pacific coast of Tohoku Earthquake and comparison with other megathrust earthquakes: Earth Planets Space, 63, pp.697–701.
31. NAMIDANCE URL: http://avi-nami.ce.metu.edu.tr , http://namidance.ce.metu.edu.tr/

ISSN 8755-6839

SCIENCE OF TSUNAMI HAZARDS

Journal of Tsunami Society International

Volume 34 Number 4 2015

FIELD SURVEY REPORT OF TSUNAMI EFFECTS CAUSED BY THE AUGUST 2012 OFFSHORE EL SALAVADOR EARTHQUAKE

Francisco Gavidia-Medina*

MARN – Ministerio de Medio Ambiente y Recursos Naturales, El Salvador

ABSTRACT

This report describes the field survey of the western zone of El Salvador conducted by an international group of scientists and engineers following the earthquake and tsunami of 27 August 2012 (04:37 UTC, 26 August 10:37 pm local time). The earthquake generated a tsunami with a maximum height of ~ 6 m causing inundation of up to 300 m inland along a 40 km section of coastline in eastern El Salvador.

** (Note: Presentation from the 6th International Tsunami Symposium of Tsunami Society International in Costa Rica in Sept. 2014 - based on the Field Survey Report of the tsunami effects caused by the August 2012 Earthquake which were compiled in a report by Jose C. Borrero of the University of California Tsunami Research Center. Contributors to that report and field survey participants included Hermann M. Fritz of the Georgia Institute of Technology, Francisco Gavidia-Medina, Jeniffer Larreynaga-Murcia, Rodolfo Torres-Cornejo, Manuel Diaz-Flores and Fabio Alvarad: of the Ministerio de Medio Ambiente y Recursos Naturales de El Salvador (MARN), Norwin Acosta: of the Instituto Nicaragüense de Estudios Territoriales(INOTER), Julie Leonard of the Office of Foreign Disaster Assistance (USAID, OFDA), Nic Arcos of the International Tsunami Information Center (ITIC) and Diego Arcas of the Pacific Marine Environmental Laboratory (NOAA – PMEL The figures of this paper are from the report compiled by Jose C. Borrero and are numbered out of sequence out of sequence from the compiled joint report. The quality of figures 2.2, 2.3 and 2.4 is rather poor and the reader is referred to the original report, as shown in the references).*

1. INTRODUCTION

El Salvador is located on the Pacific Coast of Central America bordered by Guatemala to the north and Honduras to the East (Figure 1.1). The Gulf of Fonseca at the eastern end of the country is a water body also shared by Honduras and Nicaragua. At just over 21,000 km2 and with 6 million inhabitants, El Salvador is the smallest and most densely populated country in Central America.

Figure 1.1 A political map of El Salvador. The Capital of San Salvador is indicated with a red star while red dots show the locations of the two tide stations that recorded the tsunami. Acajutla, the country's principal port in the west and La Union in the Gulf of Fonseca in the east. The area affected by the tsunami (Peninsula San Juan del Gozo) is near Acajulta.

The National Geophysical Data Center / World Data Service for Geophysics (NGDC/WDS) maintains a global historical tsunami event and run-up database. According to the database, 20 tsunamis were observed in El Salvador from 1859 to 2012, 15 of these are confirmed (validity 3-4) and 5 are questionable (validity 1-2). Nine of the sources were local, two were regional (Costa Rica, Guatemala) and nine were far field (Chile, Ecuador, Indonesia, Japan, Mexico, Russia, Alaska USA). A local tsunami in 1859 caused damage to warehouses and houses in La Union, El Salvador; a far field tsunami in Alaska 1957 caused damage to pilings in Acajutla, El Salvador. A

local event on 26 February 1902 resulted in 185 deaths, 100 injuries and houses were washed out to sea at Barra de Santiago and Barra de la Pas, El Salvador. UNESCO's Intergovernmental Oceanographic Commission (IOC) and International Tsunami Information Center (ITIC) coordinated an international post-tsunami field surveys of the tsunami and its effects. It is doing so at the request of the Governments of El Salvador (GoES). The goals include:

· Promote sharing of data with affected countries
· Minimize logistical problems for visitors and hosts
· Link visitors to country collaborators
· Provide the governments with a summary of the ITST findings

The coordination for this effort will be handled by the International Tsunami Information Center, in close coordination with the IOC and the affected country.

The Pacific Tsunami Warning Center (PTWC) issued its first information bulletin on the El Salvador event eight minutes after the earthquake at 0445 UTC on 27 August 2012 (10:45 pm local time on August 26), and upgraded its advice to a tsunami warning for Central America countries at 0458 UTC as a precaution based on strong indications that this event was a slow "tsunami" earthquake.

Instrumental data recorded at sites in El Salvador showed a tsunami with 14 cm amplitude at Acajutla to the north at 12:10 am local time (0610 UTC) and no clear tsunami signal at La Union in the Gulf of Fonseca. There were, however, no gauges along coasts closest to the epicenter. The warning was cancelled at 0627 UTC when there was no expectation of new destructive impacts outside the area already potentially affected.

About 3 hours after the earthquake, sea level recordings from the Galapagos Islands showed a tsunami signal with amplitude of 40 cm. This indicated that a significant tsunami had been generated, even if its main impact was only localized near the epicenter. No reports came out of El Salvador in those first few hours of any damaging or destructive tsunami activity.

Within El Salvador however, there were reports of tsunami waves on the night of 26 August (local time) that were brought to the attention of government scientists at MARN (Ministerio del Medio Ambiente y Recursos Naturales) in San Salvador. On the basis of these reports, a preliminary survey was conducted in the field on 27 August by scientists from MARN. The preliminary survey established that a tsunami did occur and primarily affected the Peninsula of San Juan del Gozo, a sparsely populated area located directly shoreward of the epicenter. This survey also determined that there were no deaths caused by the tsunami but that there were several injuries caused by the wave.

2. EARTHQUAKE AND TSUNAMI

On 26 August 2012 at 10:37 pm local time (27 August, 2012, 0437 UTC), an earthquake with magnitude 7.3 (USGS) occurred off the coast of El Salvador. The earthquake epicenter as reported by the USGS was located some 100 km due south of the coast, in-line with the entrance to

Jiquilisco Bay (Figure 2.1). As shown in the regional bathymetry (GEBCO), the earthquake source region is in the vicinity of the Central America Trench where water depths range from 4000 to 5000m. The principal axis of a canyon-like bathymetric feature is oriented with the San Juan del Gozo Peninsula. Approximately 50 aftershocks with magnitudes between 4.2 and 5.5 occurred in the vicinity of the main event between 27 August 27 and 11 September 2012.

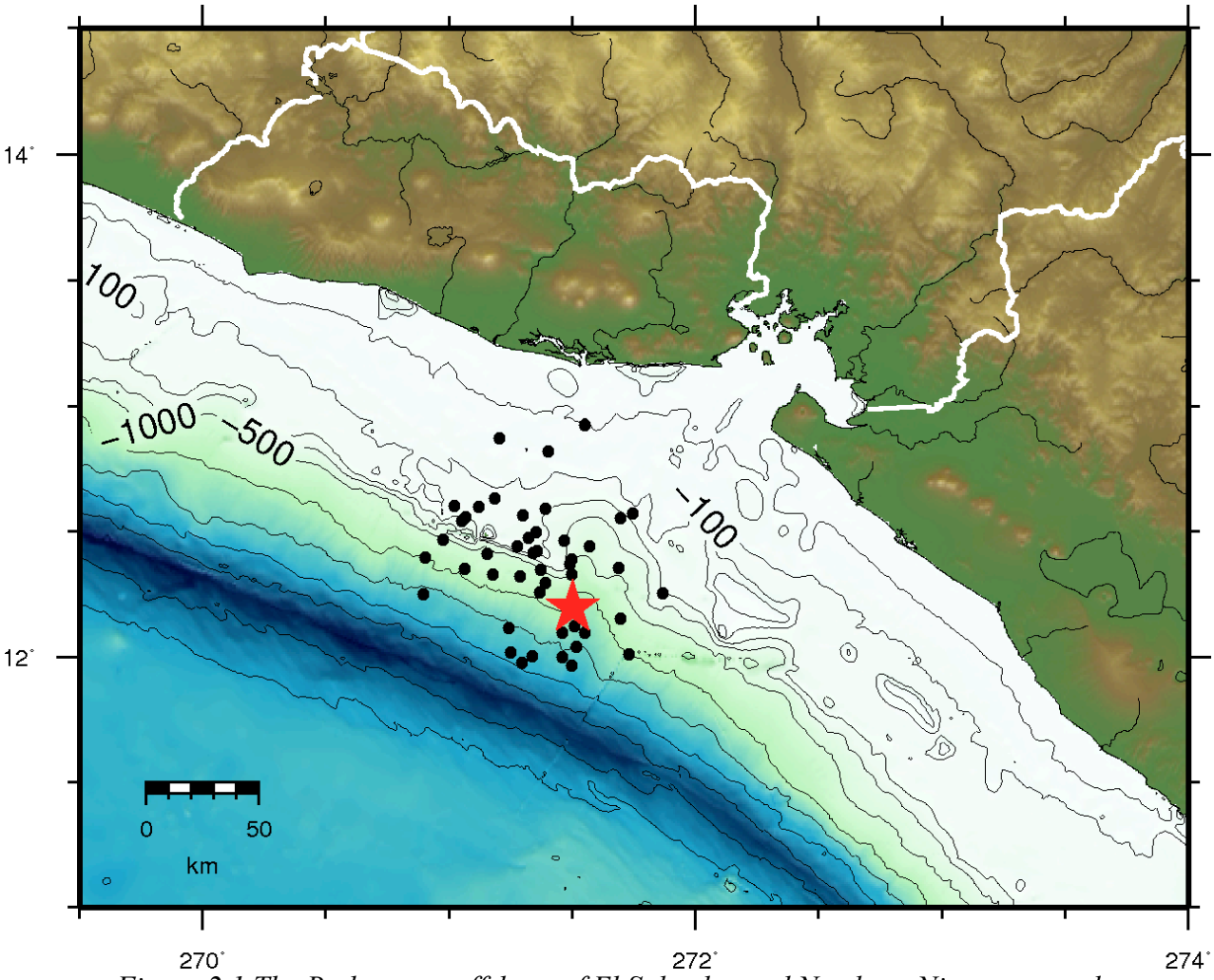

Figure 2.1 The Bathymetry offshore of El Salvador and Northern Nicaragua and the location of the USGS defined earthquake epicenter (red star). Black dots correspond to epicenters of aftershocks through 11 September, 2012. Contours labeled in meters.

The initial assessment of the earthquake by staff of the Pacific Tsunami Warning Center (PTWC) determined that the earthquake was significant due to the magnitude of the strength of the seismic signals and the long period nature of the initial seismic waves. Within 10 minutes of the main shock, additional analysis by the PTWC suggested that the earthquake could be characterized as a 'slow' earthquake. This was indicated by values (; Newman and Okal, 1998) in the range of -6.5 to -6.0 as computed by the PTWC. Typical values of for 'normal' thrust earthquakes are generally larger, in the range of -4.7. Additionally, values derived by the West Coast Alaska Tsunami Warning Center (WCATWC) were even lower at -7.0, further suggesting a very slow event.

Finally, analysis by the USGS finite fault method released in the days after the earthquake confirmed the slow nature and extended duration of the earthquake source, this is shown in the energy release function reproduced in Figure 2.2. This Figure shows that the energy released from this event occurred over a time period of approximately 70 seconds, which is quite long for an earthquake of that magnitude.

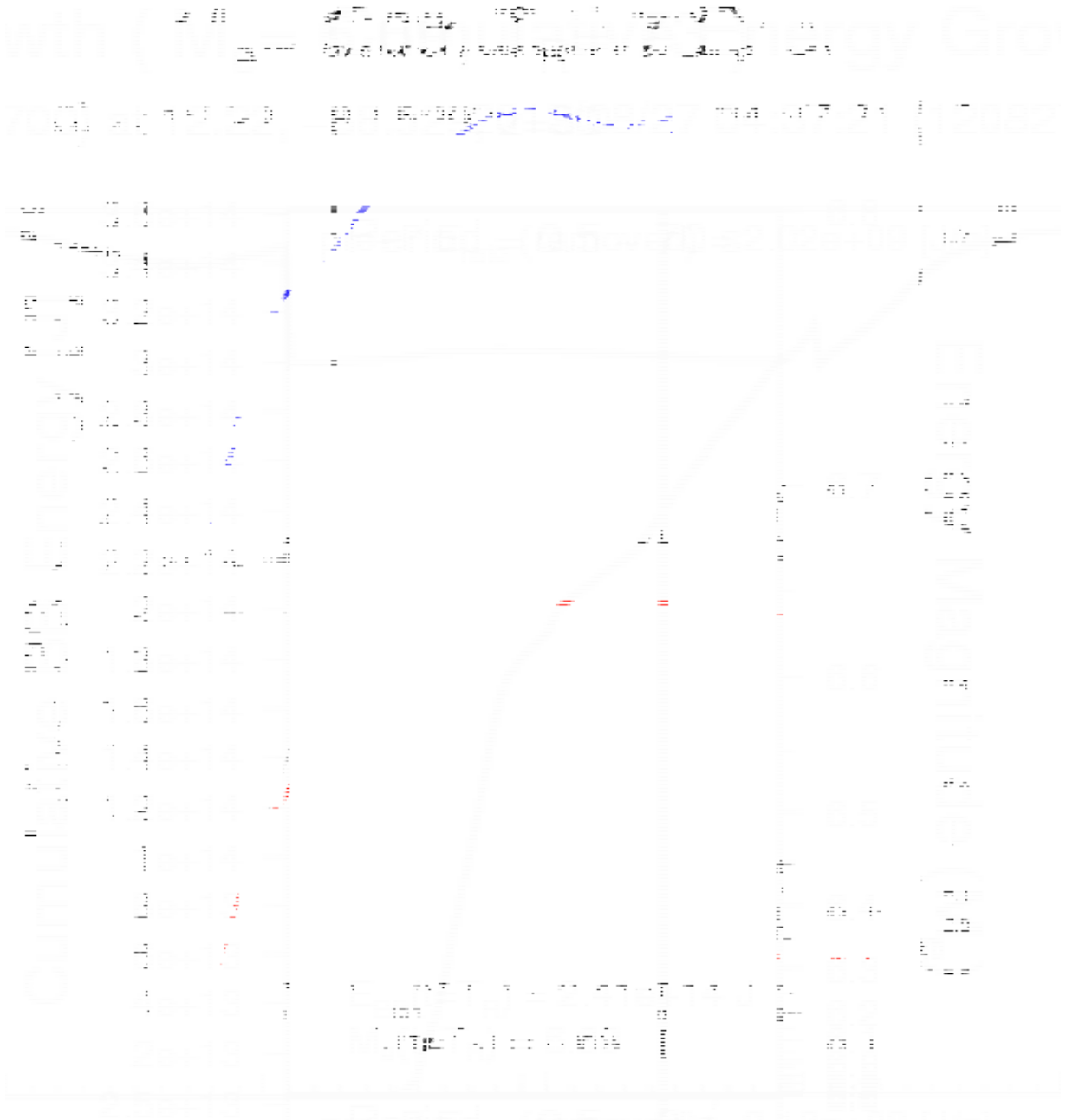

Figure 2.2 The preliminary energy-time relationships produced by the Real-Time Earthquake Energy and Rupture Duration Estimate project of the Georgia Institute of Technology and emailed to a distribution list approximately 10 minutes after the earthquake.

The tsunami was observed instrumentally on both near and far field water level recorders. In the near field the tsunami was observed on the Acajutla and La Union, El Salvador tide gauges. In the far-field, the tsunami was observed on tide gauges in the Galapagos Islands, La Libertad, Ecuador and on DART station 43413 (Table 2.1 and Figure 2.3 – 2.9).

Table 2.1 PTWC Summary of tide gauge recordings from the El Salvador tsunami.

Station	Country	Latitude	Longitude	arrival	P2T	Period
		(deg)	(deg)	(hrs)	(m)	mm:ss
Acajutla	El Salvador	13.57	-89.84	0:52	0.21	8:00
La Unión	El Salvador	13.31	-87.81	1:40	0.04	9:00
Baltra	Ecuador (Galápagos Island)	-0.44	-90.28	2:30	0.70	10:00
Santa Cruz	Ecuador (Galápagos Island)	-0.72	-90.31	2:49	0.39	13:20
La Libertad	Ecuador	-2.22	-80.91	3:36	0.37	11:30
DART 43413	n/a	10.84	-100.08	1:36	0.02	8:00

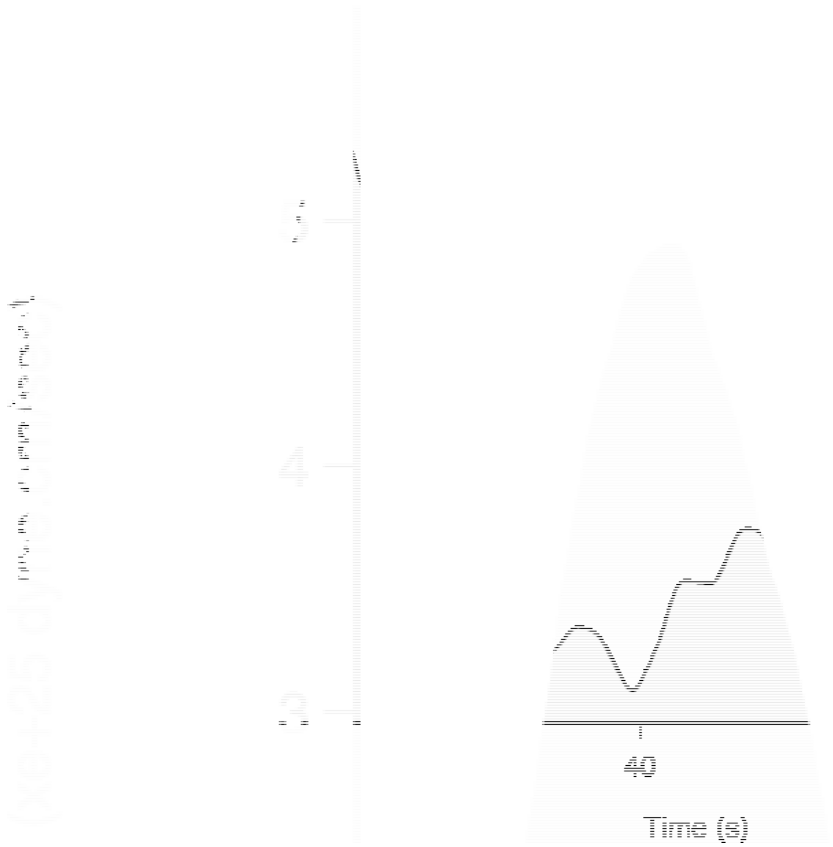

Figure 2.3 Energy release function for the 27 August 27 2012 El Salvador earthquake (Mw 7.3). Energy release occurs over 70 seconds.

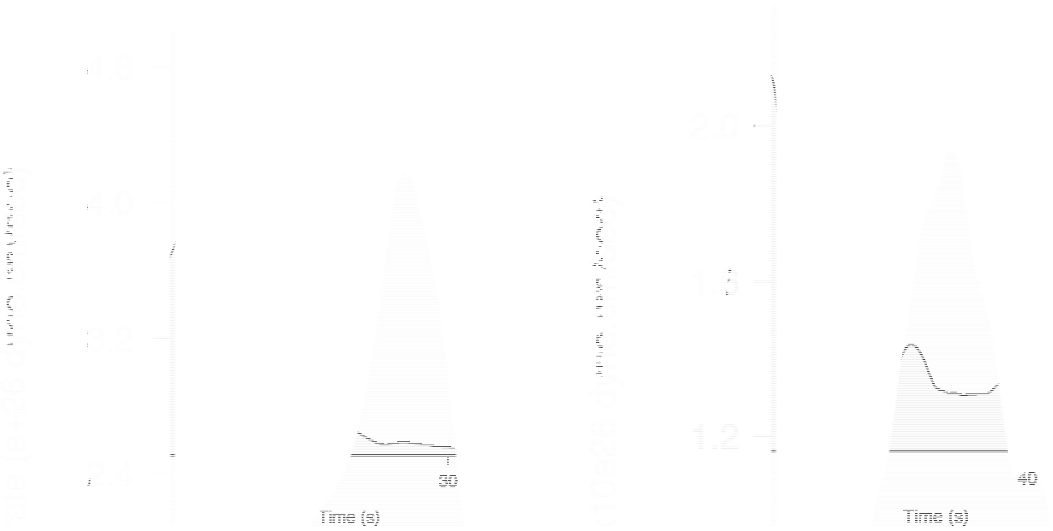

Figure 2.4 Energy release functions for the 31 August 2012 Philippines earthquake (Mw 7.6, left) and the 5 September 2012 Costas Rica Earthquake (Mw 7.6, right). Note that although both of these are larger in terms of magnitude, the energy is released in less time than in the El Salvador event, particularly in the case of the Philippines event.

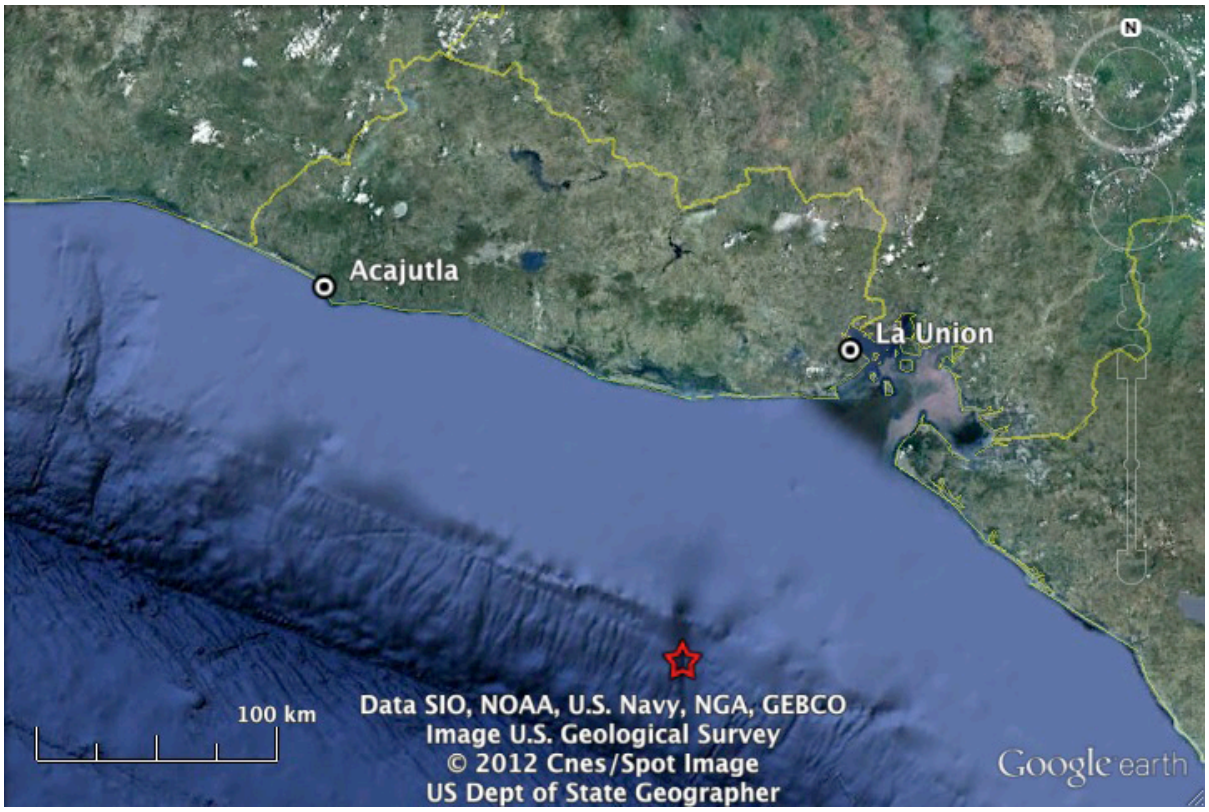

Figure 2.5 Locations of the two tide stations in El Salvador that recorded the August 26th, 2012 tsunami. The earthquake source location is indicated with the red star.

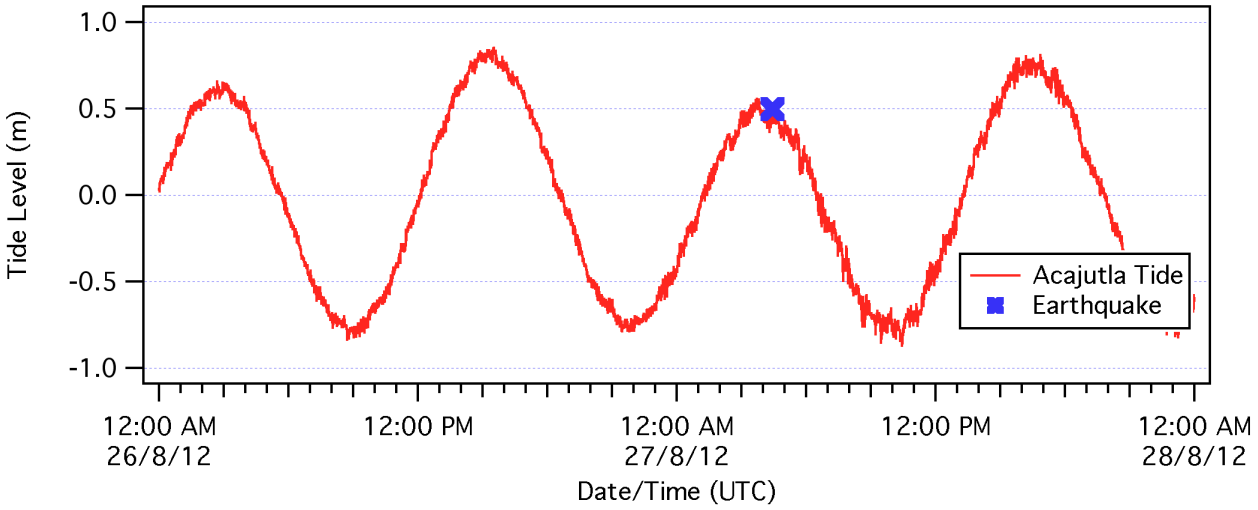

Figure 2.6 Acajutla tide gauge data from the time of the earthquake.

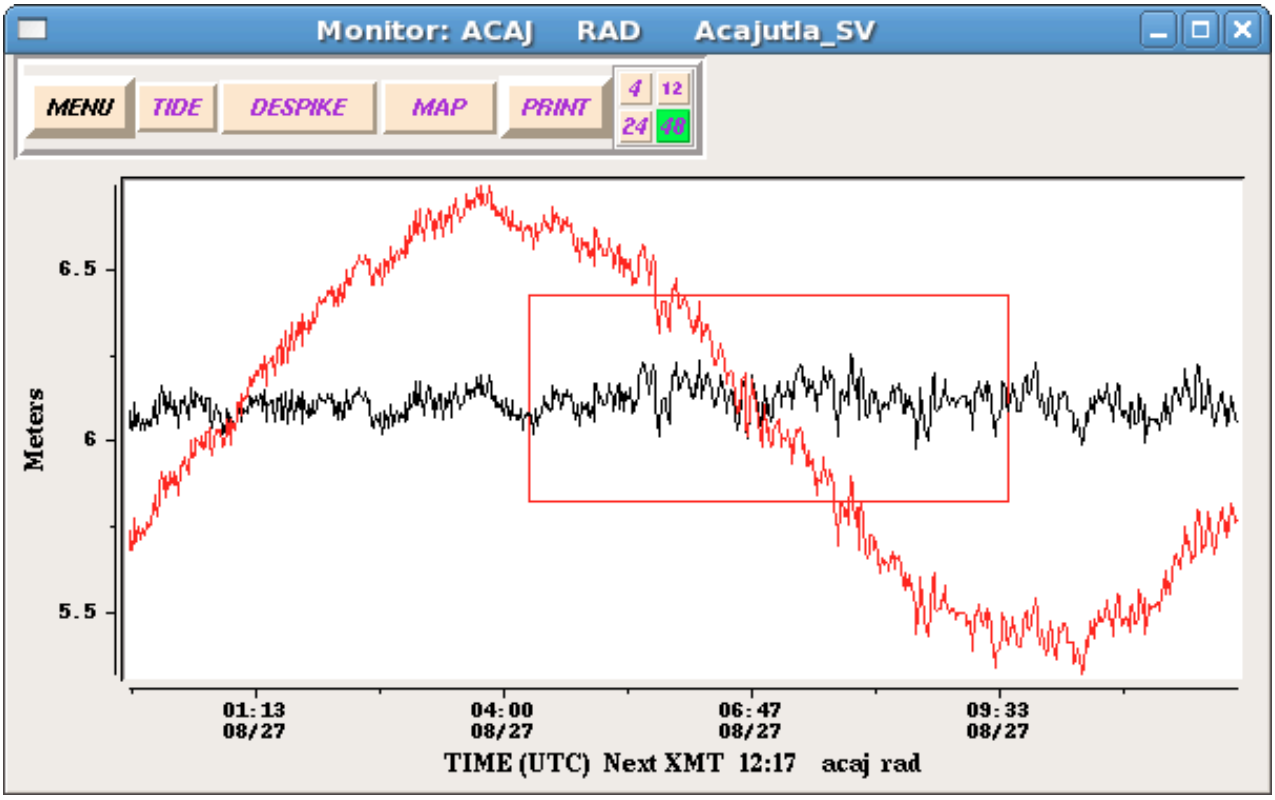

Figure 2.7 PTWC plot of the El Salvador tsunami on the Acajutla, El Salvador tide gauge.

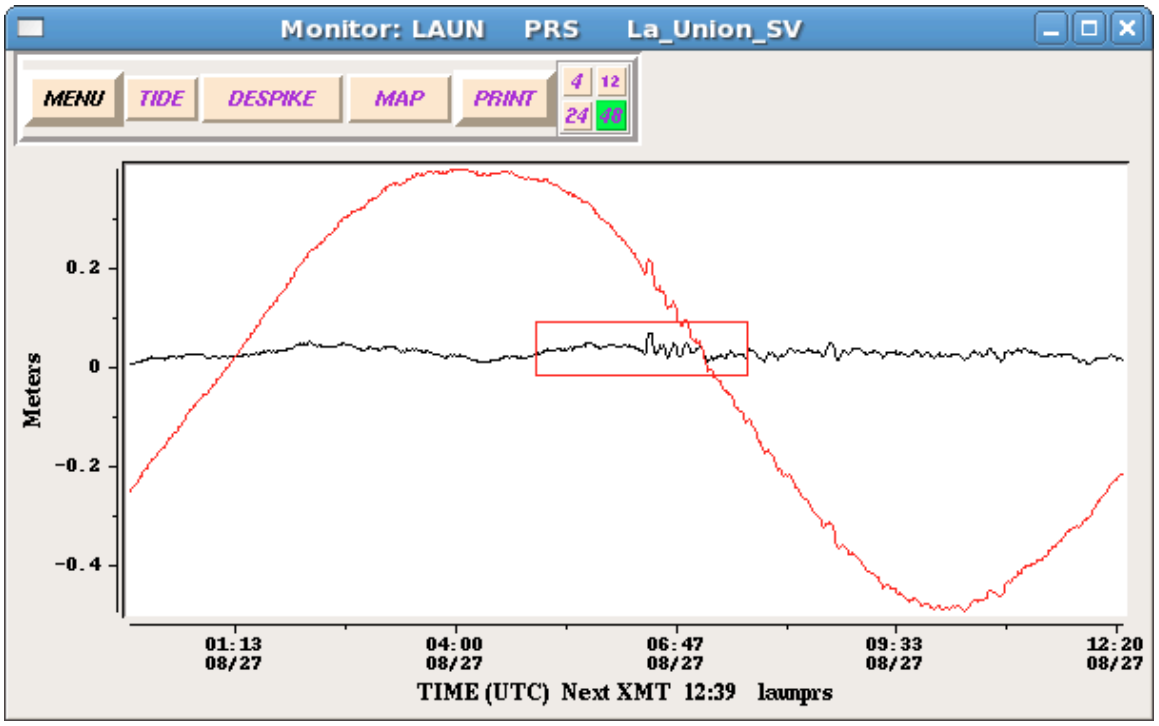

Figure 2.8 PTWC plot of the El Salvador tsunami on the La Union, El Salvador tide gauge.

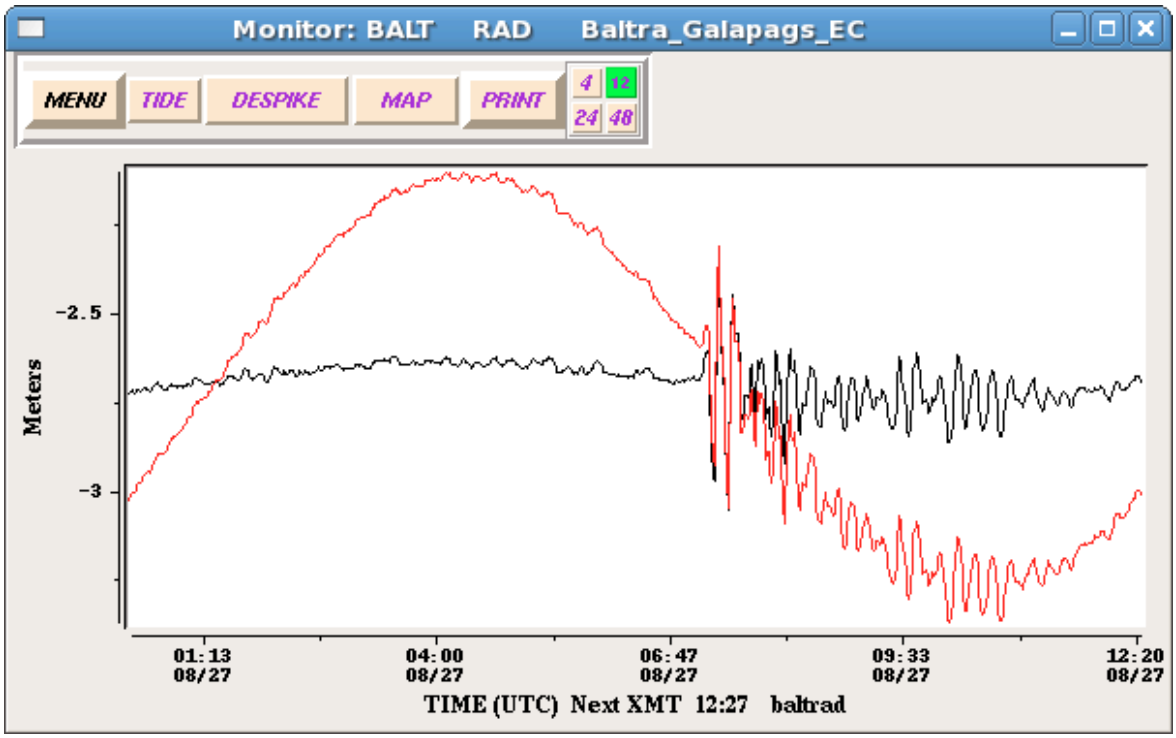

Figure 2.9 PTWC plot of the El Salvador tsunami on the Baltra, Galapagos Islands tide gauge. The gauge is located ~1400 km away along a 191° path.

Due to the location of the earthquake and the fact that tsunamis radiate the majority of their wave energy perpendicular to the axis of the fault plane, neither of the El Salvador gauges were ideally located to receive the tsunami signal. Furthermore, Acajutla is located on the far side of a large headland while La Union is located several kilometers from the open ocean in the Gulf of Fonseca. In contrast, the Galapagos Islands are nearly ideally located to receive a strong signal from this event. Although they are approximately 1400 km away, they are located on a 190° path (S) from the source region, just 15° off of the trench perpendicular direction of 205° path (SSW), and favorably situated for energy focusing by the Cocos Ridge. As a result the two stations in the Galapagos (Baltra and Santa Cruz) recorded a very strong, clear tsunami signal that arrived some 2.5 hours after the earthquake. Following the initial wave packet, both stations also responded with a secondary (and in the case of Santa Cruz tertiary) wave packet with amplitudes nearly as large as the initial wave. A similar extended duration and resurgence of wave height was also observed on these stations during the March 11, 2011 Tohoku tsunami (Lynett et al., 2012).

Further off axis, were DART 43413, approximately 1200 km away at 265° path (W), and the La Libertad, Ecuador station, approximately 1800 km away at 155° path (SSE). Evident in the DART record is the high frequency signal from the earthquake followed ~1.5 hours later by a single tsunami wave pulse with a peak to trough (P2T) height of 0.024 m. The La Libertad signal is characterized by long period non-tsunami oscillations present before the tsunami arrival. The tsunami itself appears clearly some 3.5 hours after the earthquake, with the largest signal occurring some 5 hours after the tsunami arrival.

Within days of the event preliminary hydrodynamic models of the tsunami had become available. Results from the MOST tsunami model (Titov and Gonzalez, 1997) are presented in Figure 2.10 (Nikos Kalligeris, pers. comm.). For this simulation, the model was initialized using the USGS finite fault solution for the slip distribution. The finite fault solution describes a distributed slip distribution across the source area with a maximum slip amount on the order of 1 m. While the model result shows strong focusing of wave energy towards the western end of the San Juan del Gozo peninsula, the absolute wave heights are somewhat deficient to have caused the reported 5 m tsunami heights in that area. The model also shows some focusing of wave energy towards the east in to northern Nicaragua and corresponding with areas that reported some tsunami effects.

The fact that the direct application of the USGS Finite Fault model as the initial condition for the tsunami hydrodynamic yields results deficient in wave heights necessary to explain the reported effects should not come as a surprise. Indeed, in the case of the October 2010 Mentawai earthquake and tsunami, hydrodynamic simulations initialized with a direct application of the finite-fault slip amounts also severely under predicted the observed wave heights (Hill et al., 2012). In order to match the observed wave effects, it was necessary to scale the slip amounts by an average value of 5.6 (Newman et al., 2011). The necessity for this scaling factor was attributed to the slow, shallow nature of the earthquake rupture and the correspondingly lower shear wave velocities encountered in the shallower portions of the earth's crust (Newman et al., 2011).

3. TSUNAMI FIELD SURVEY

An initial survey was conducted by representatives of MARN, the Salvadorean Ministry for the Environment and Natural Resources (Ministerio del Medio Ambiente y Recursos Naturales) in the days immediately following the event (on 27 – 29 August 2012). This survey focused on attending to the immediate needs and disseminating factual information to the affected population. A number of interviews were recorded from eyewitnesses.

Following the organization of the International Tsunami Survey Team (ITST), a second survey visited the affected areas on 5-7 September 2012. The survey team visited 11 separate sites throughout the affected area. These sites are depicted in Figure 3.1.

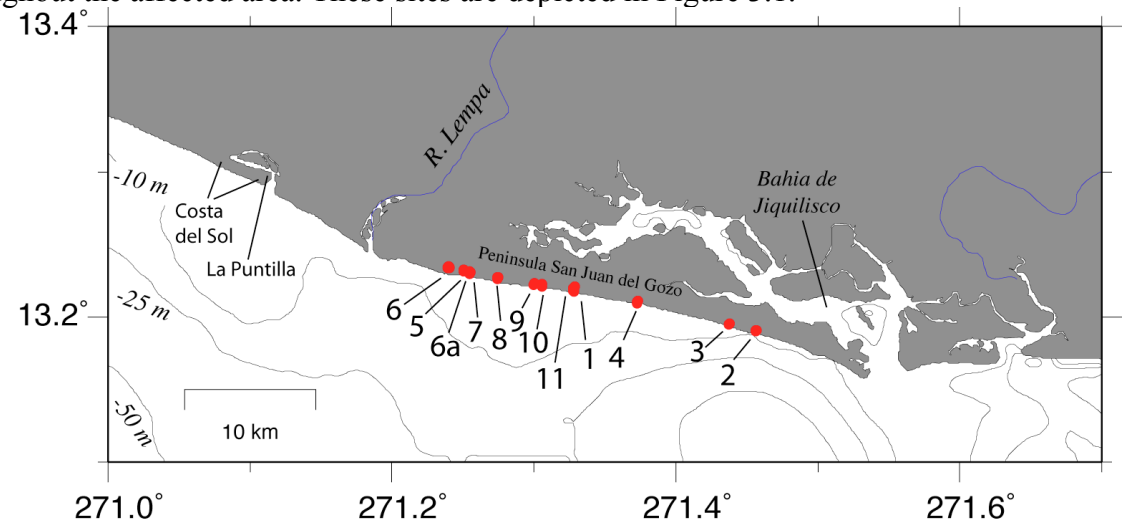

Figure 3.1 Survey sites along the San Juan del Gozo peninsula.

The survey focused on the San Juan del Gozo Peninsula where the strongest tsunami effects were observed. At each of the 11 sites one or more measurements of tsunami height, runup, flow direction and inundation distance were recorded using established protocols (Synolakis and Okal, 2002, Dominey-Howes et al., 2012). Watermarks were surveyed with a Trimble GPS rover connected via Bluetooth to a laser range finder (Lasercraft XLRic) to record offset points and differentially corrected during post-processing with the base station network of UNAVCO. Measured data are presented relative to the tide level at the time of tsunami arrival.

Table 3.1 Survey site names corresponding to numbers in Figure 3.1.

Number	Site Name (closest town or between towns)
01	La Maroma
02	Corral de Mulas (1)
03	Corral de Mulas (2)
04	El Retiro
05	Isla de Méndez (1)
06	Montecristo mangrove
6a	Isla de Méndez (2)
07	Isla de Méndez (3)
08	San Juan del Gozo lagoon
09	Ceiba Doblada (1)
10	Ceiba Doblada (2)
11	Ceiba Doblada (3)

The definitions of reference water level, inundation distance, flow depth, tsunami height and run-up height are as follows:

1. Reference water level: Is the tide level at the time of tsunami arrival.
2. Inundation distance: Is the horizontal distance wetted by the tsunami flow.
3. Flow depth: Is the depth of the tsunami surge above the ground as indicated by flow markers.1
4. Tsunami height: Is the sum of flow depth and the local topographic height.

(Flow markers: piles of debris; impact scars on tree trunks; bark stripped from trees; mud marks on the walls of buildings).

4. RUN-UP HEIGHT ABOVE SEA LEVEL REACHED BY THE TSUNAMI AT THE POINT OF MAXIMUM INUNDATION.

All of the sites surveyed in El Salvador were located on the San Juan del Gozo peninsula which separates Jiquilisco Bay from the Pacific Ocean. In total 11 sites were surveyed as indicated in Figure 3.1. All of the sites were very similar in terms of the geomorphology characterized by a relatively steep, dark sand beach face, with a dune crest at the top of the beach berm. Landward of the beach berm the terrain was either level or sloping slightly downward. The vegetation was comprised of low beach plants, sea grape (icacos) plants, grasses and spiny cactus type plants. There were very few tall trees only at the western extreme of the peninsula (Montecristo mangrove).

Site 01: La Maroma.

It is name of the town nearest of a section of the beach along the San Juan del Gozo Peninsula. It was in this area however where the most people were affected by the tsunami and the strongest effects were observed. This area is also the site of one of larger sea turtle hatcheries (vivero) in the area.

Ofilio Herrera, MARN and Civil Protecion, indicated that the peninsula lacked high ground to evacuate to, and few means of transportation for moving inland. Mr. Herrera said communities on peninsula did not receive any tsunami alert prior to the arrival of the tsunami.

We were met at site by the municipal Mayor (Alcalde), Mr. Rigoberto Herrera Cruz. He was accompanied by several representatives from the local Civil Protection group and turtle hatchery workers.

The site featured a small shed (ramada) with wood posts and the walls and roof made from aluminum siding (lamina) located next to the hatchery. The hatchery itself is a simple structure comprised of perimeter fence with concrete posts. Wooden posts supported a simple roof made of palm fronds for shade.

During the tsunami, the walls of the ramada were torn off of the posts that are deeply embedded in the sand. The posts themselves were not pulled out of the ground, but some were leaned over by the force of the water. By the time of the survey the ramada had been repaired and had new walls and roof.

A worker at the hatchery, Jose Barrera-Garcia, was in the ramada as the tsunami struck and came out when he heard people crying out. He was dragged some 90 m by the wave from the ramada to a tree, where he was suspended in tree branch. The height of the branch was measured at ~2.1 m above ground. Mr. Barrera-Garcia reported that he saw three waves, however we suspect there is some confusion in differentiating between wind and tsunamis waves. Mr. Barrera-Garcia said it took 20 minutes for water to recede and fully drain. He said flow depth reached just beneath the roof of the ramada as indicated in Figure 3.5. At maximum inundation extent observed (340 m) by Mr. Garcia, he said less than 1 m water depth.

Figure 3.5 Jose Barrera-Garcia at the newly rebuilt ramada. Mr. Barrera-Garcia was swept away by the tsunami and suffered minor injuries. The tsunami flow depth at this location was reported by Mr. Barrera-Garcia to be over 2 m.

Jose Fermin Piñeda, 25 years old, from Isla de Mendez, was on the beach when the tsunami arrived. He had just delivered a turtle to the hatchery. He was standing just outside the shed that Jose Barrera- Garcia was sitting in. He also described 3 waves, the first of which carried him beyond the tree that Jose Barrera was caught in, near the bushes.

Jose Gabriel Chavez, local coordinator for Civil Protection, said he was inland and felt the earthquake describing it like he was in a swaying boat. He felt the swaying for 30-40 seconds. He said when he arrived at the impacted area (turtle hatchery referenced above) he found ~40 people injured, 3 of which are still in hospital. He also described gurgling noises (water draining into sand) on the beach area.

Jose Maria Argueta, local Civil Protection worker and member of local NGO Asociación Mangle that is working with Save the Children a USAID/OFDA-funded disaster risk management project, said that at the organizational level the Civil Protection personnel had basic tsunami knowledge but needed more support and training. Training by the project has covered first aid and early warning for flooding events up to now. Mr. Arqueta indicated the local population had no knowledge about tsunamis and did not know it was a hazard in their area. Mr. Arqueta stated that no one in Isla de Mendez received a tsunami alert, but that the community passed the information about the wave(s) up the chain to the next level, which was the municipality of Jiquilisco.
Site 02: Corral de Mulas (1).

After Isla de Mendez the team moved towards the eastern end of the Gozo Peninsula, stopping at three locations while driving along the beach dunes. At the first site we spoke with Jaime Enrique Mejia, a worker at turtle hatchery who was not at site at time of event. However, he showed us debris (tree trunk and palms) that were deposited just in front of a hut used by workers. The hut was not impacted. At the time of the earthquake, Mr. Mejia was inland and reported that he felt the earthquake, which he described as light (‘leve’ in Spanish). He reported that light fixtures hanging from the ceiling swayed during earthquake and that corrugated sheet metal ("lamina") used for walls and roofing vibrated strongly.

Site 03: Corral de Mulas (2).

Francisco Esteban Elena Aguilar, turtle hatchery worker said that the shaking lasted 2-3 minutes. He describes two waves, second being the largest. Aguilar mentioned his goods and personal items stored in the hut were lost. He also mentioned that water reached the top of nearby fence post, measured at ~1 m higher than the dune crest and a few meters inland.

Site 04: El Retiro

No witnesses were encountered at El Retiro, however a resident of the area working with the survey team (Mr. Ofilio Herrera) reported that at this location a child as well as a man and a horse were dragged down the beach by the wave. At this site the team encountered evidence of tsunami over-wash and inundation.

Site 05, 06, 6a, 07: Isla de Mendez (1), (2), (3) and Montecristo mangrove.

Montecristo mangrove is located to the west of Isla De Mendez (see Figure 3.1). This marks the beginning of a forest of tall mangroves that extends approximately 6 km to the west towards the mouth of the Rio Lempa. The mangroves at the shoreline are dying off as evidenced by the brown color and seen in overhead images. The exact cause of the mangroves dying off is not known, however it is a slow, ongoing process and is not related to the tsunami.

Witness Evan Antonio Coronel was sitting near the shed area at the time of wave arrival. He described three waves, the third of which carried him inland. Mr Coronel indicated the furthest inundation point, ~150 m from the shoreline. His testimony of the effects indicated a maximum of ~4.5m flow depth. He also indicated a loud noise preceding wave arrival which he described as like a loud bus. Another local resident, Carlos Antonio mentioned that there were approximately 50 people working on that part of the beach on the night of the tsunami. He himself was in the community of San Juan del Gozo lagoon that evening, and didn't feel the tremor. They did not receive a warning. He said that 6 turtle nests were lost. From this location, the survey team walked approximately 1 km further west to the edge of the dead mangrove forest. In this area there was evidence of tsunami inundation. A run-up point and inundation distance were measured.

Site 08, 09, 10, 11: Ceiba Doblada (1), (2), (3) and San Juan del Gozo lagoon.

Driving eastward towards Ceiba Doblada, the team stopped at several sites where there was clear evidence of tsunami inundation. There were no residents or locals in the area available for interviews. At these sites the teams measured run-up and inundation and documented the evidence of the tsunami (Figure 3.26 through Figure 3.28).

Figure 3.26 Tsunami debris line.

Figure 3.27 Tsunami debris line.

Figure 3.28 Dead vegetation from salt water intrusion.

During the helicopter over flight of the following day, several aerial images of this area were recorded (Figure 3.29 and Figure 3.30).

Figure 3.29 Aerial view of a tsunami debris line.

Figure 3.30 Aerial view of sand deposits from tsunami overwash.

To the west of the study area is a popular and highly developed beach resort area known as Costa del Sol (see Figure 3.1). At the eastern end of this area is a grouping of restaurants built directly on the water front. Indeed some of the restaurants have seating areas set directly over the water (Figure 3.31 and Figure 3.32). Given the extremely vulnerable location of these structures, it could reasonable by expected that if a tsunami wave the same size as that which affected Isla de Mendez hit this area, there would have been reports of significant effects or damage.

Figure 3.31 La Puntilla.

Figure 3.32 La Puntilla.

During the initial survey immediately after the earthquake and tsunami conducted by MARN, residents and proprietors here did not report any such effects, nor was any evidence observed supporting that notion. Only at the isla Tasajera, between Costa del Sol and rio Lempa, the turtle hatchery workers report that they hear something unusual coming from the sea, but no evidence of the tsunami was find it.

Just to the west of La Puntilla is the popular resort area of Costa del Sol (Figure 3.33 through Figure 3.35).

Figure 3.33 Costa del Sol.

Figure 3.34 Costa del Sol.

Figure 3.35 Aerial view towards La Puntilla and Costa del Sol to the west.

As seen in the aerial images, the area is very developed with numerous structures built close to shore and many potential witnesses in the area on the night of the tsunami. During the preliminary MARN survey, there were no reports from this area of inundation, damage or effects, again suggesting that the tsunami here was very small.

The preliminary MARN survey received reports from several other areas around El Salvador regarding the tsunami.

At the Port of Acajutla, there were no observations of sea level changes and ships moored in the port did not experience any unusual surges. We note that a surge of 0.2 m with an 8 minute period was recorded on the Acajutla tide gauge (Table 2.2). Workers at the port maintained their normal shifts, however they were alerted to the possibility of tsunami effects that night by MARN.

Playa El Espino is located to the east of the entrance to Jiquilisco Bay. Resident and president of the local Restaurants Association Mrs. Blanca Yorahimi Larreynaga was interviewed by telephone on the morning after the tsunami. She reported that there were no observable tsunami effects and that the local police had moved into the peninsula of St. Juan del Gozo to help assist people affected in that area.

Playa El Cuco is located well to the east of the Bay of Jiquilisco. A phone call was placed to the administrators of the Hotel Las Flores, a popular surfing resort for North Americans. They reported that on the night of the tsunami there were no unusual events. The local surf guide and boat captain said that the boats left parked on the beach were not moved or disturbed in any way and that activities of the next day resumed normally.

The data collected by the El Salvador survey team is summarized in Figure 3.32, Table 3.2 and Table 3.3. The data are divided into flow depths, tsunami heights and runup heights as defined in Figure 3.3. Because the topography landward of the dune ridge sloped downward, runup heights are generally lower than the maximum tsunami heights.

Table 3.2 Run-up measurements from the 2012 El Salvador tsunami.

Date	Time	Latitude	Longitude	Run-up*	Watermark	Description
	UTC-6	North	East	(m)		Eyewitness confirmed
5-sep-2012	12:05:34	13.221	-88.671	2.20	Wrack Line	Yes
5-sep-2012	15:15:09	13.191	-88.543	5.35	Wrack Line	On top of dune tree log
5-sep-2012	15:46:52	13.195	-88.562	3.69	Wrack Line	Brown grass
5-sep-2012	16:38:15	13.211	-88.627	1.66	Wrack Line	Yes
6-sep-2012	08:32:22	13.232	-88.749	2.08	Wrack Line	Brown vegetation
6-sep-2012	08:56:52	13.232	-88.749	2.30	Wrack Line	Brown vegetation
6-sep-2012	10:01:02	13.235	-88.760	2.14	Wrack Line	Embankment next to mangrove
6-sep-2012	10:06:42	13.235	-88.760	1.91	Wrack Line	Next to mangrove
6-sep-2012	10:54:07	13.231	-88.745	3.51	Wrack Line	Field next to fence
6-sep-2012	10:58:39	13.231	-88.745	3.50	Wrack Line	Field next to fence
6-sep-2012	11:18:21	13.227	-88.725	3.30	Wrack Line	Field next to fence
6-sep-2012	11:24:57	13.227	-88.725	3.07	Wrack Line	Brown vegetation
6-sep-2012	12:27:27	13.223	-88.700	3.22	Wrack Line	Brown vegetation
6-sep-2012	12:47:18	13.223	-88.694	2.07	Wrack Line	Brown vegetation
6-sep-2012	13:03:53	13.220	-88.672	3.17	Wrack Line	Brown vegetation

*The run-up average was 2.88 m.

Date	Time	Latitude	Longitude	Terrain	Flow depth	Tsunami height*	Watermark	Description
	UTC-6	North	East	(m)	(m)	(m)		Eyewitness confirmed
5-sep-2012	11:42:07	13.218	-88.672	4.22	2.1	6.32	Mud line inside	House pole
5-sep-2012	11:53:35	13.219	-88.672	3.54	2.3	5.84	Broken branch	Wrapped in sheet metal
5-sep-2012	15:51:40	13.195	-88.562	5.13	0.5	5.63	Dune overtopped	Yes
5-sep-2012	16:34:33	13.210	-88.627	3.97	0.5	4.47	Damage trim line	Wooden palm leef hut
6-sep-2012	08:26:22	13.232	-88.749	3.25	1.6	4.85	Damage trim line	Hut with sheet metal
6-sep-2012	08:48:35	13.232	-88.749	3.29	1.6	4.89	Damage trim line	House siding
6-sep-2012	09:14:16	13.232	-88.749	2.19	0.5	2.69	Raft debris	Debris in fence
6-sep-2012	09:46:06	13.234	-88.759	3.55	0.6	4.15	Damage trim line	Hut with sheet metal
6-sep-2012	10:59:56	13.231	-88.746	3.19	1.6	4.79	Broken branch	Tree on top of dune

*The tsunami height average was 4.85 m.

4. SUMMARY, FINDINGS AND NEXT STEPS

A tsunami was generated by the 26 August 26 2012, magnitude (Mw) 7.4 earthquake centered offshore of south eastern El Salvador. The causative earthquake was a 'slow earthquake', a type of earthquake known to cause tsunamis disproportionally higher than the earthquake magnitude alone would suggest. The tsunami generated by the earthquake primarily affected approximately 30 km of the El Salvador coastline directly landward of the earthquake epicenter.

The strongest tsunami effects were observed along the beaches of the San Juan del Gozo peninsula which runs eastward from the mouth of the Lempa River and separates Jiquilisco Bay from the Pacific Ocean. Peak tsunami heights were measured up to 6 m at Isla de Mendez with tsunami heights of 3 to 6 m measured approximately 15 km west and east of this location. The tsunami caused inundation of up to 350 m inland at Isla de Mendez. Tsunami heights were relatively uniform across the survey area. Coastal areas 25 km to the west (i.e. Costa del Sol) were not affected by damaging tsunami waves, nor were areas just to the east, suggesting relatively localized effects.

In addition to the Field Survey, ITST team members were also requested to provide advice to MARN on how to strengthen its national tsunami warning and mitigation system. The

observations and findings from the ITST team were supplemented with advice from Directors of the Pacific Tsunami Warning Center and International Tsunami Information Center, and the Technical Secretary of the ICG/PTWS. The findings should be considered preliminary. Further detailed discussions with subject matter experts will be necessary to develop action plans that can lead to robust and reliable improvement to El Salvador's tsunami warning and mitigation system. The overall findings were as follows:

1. The 26 August 2012 earthquake highlighted the insufficiency of current El Salvador seismic resources to rapidly and accurately determine the magnitude of a great earthquake in time to identify the risk of an impending tsunami and allow authorities to act on that information. Denser national and regional seismic networks and quick magnitude estimation techniques will be required for timely local earthquake source characterization. In the interim, MARN may want to utilize the PTWC Earthquake Observatory Message as a first indicator of earthquake size.

2. MARN should review of their existing tsunami alert and warning protocols, particularly for near-field events. For local tsunamis and immediate alert dissemination in minutes, warnings should be based solely on earthquake information since seismic signals are currently the fastest early tsunami warning signals.

3. To determine the severity and longevity of dangerous tsunami waves, real or near-real time monitoring of sea levels is required. Currently, El Salvador has 2 working coastal sea level stations and Nicaragua 1 coastal sea level station. More are required, especially facing the open ocean, and should be given highest priority as the most economical means of confirming tsunamis. Actual observations, whether by coastal or deep-ocean sensors, along with eyewitness reports by local authorities, are essential for determining when to cancel tsunami warnings, and when it is safe for the public to return to the evacuated area.

4. At present, local tsunami wave forecasting must utilize database-driven pre-calculated tsunami scenarios. In general, near real-time data, whether by DART systems or coastal gauges, are too late to be used as input to local tsunami wave forecasting. Deployment of a deep-ocean sensor off El Salvador will be of most use to countries around the Pacific monitoring a Central America source as a distant tsunami that might impact them.

5. To enable communities to better respond to local tsunamis, they must know their tsunami hazard and what to do. Development of tsunami inundation maps and evacuation zones for at-risk areas of El Salvador will assist greatly. Additionally, outreach and education are essential activities. Place emphasis on the recognition of a tsunami's natural warnings signs as a key local tsunami preparedness message. Development and mainstreaming tsunami preparedness into school curricula will ensure sustainability over generations.

6. Civil Protection should develop tsunami response plan at the national level, as well as the local level. Response plans should document agencies, protocols, and standard operating procedures to enable rapid and seamless warning communication and evacuation of vulnerable communities, followed by immediate disaster response to save lives.

7. To focus on the tsunami hazard, a national-level tsunami coordination committee comprised of key stakeholder agencies should be formed to regularly meet to discuss, agree, and oversee the development on sustainable, effective end-to-end warning system. Topics should include (1) hazard risk assessment, (2) warning, (3) emergency response, and (4) preparedness and mitigation.

8. Identify a sustainable source for tsunami information and technical assistance. Technical assistance on (1) hazard risk assessment, (2) warning, (3) emergency response, and (4) preparedness and mitigation is available from several sources including but not limited to technical cooperation agencies like JICA, GIZ, USAID, or others, intergovernmental mechanisms like the ICG/PTWS and its International Tsunami Information Center ITIC and from UN agencies like UNDP, UNESCO and ISDR. These should be considered as subsidiary to internal capacities El Salvador is trying to develop to address and mitigate tsunami risk.

5. REFERENCES

Abe, K., Tsuji, Y., Imamura, F., Katao, H., Iio, Y., Satake, K., Bourgeois, J., Noguera, E., and Estrada, F. (1993) Field Survey of the Nicaragua Earthquake and Tsunami of September 2, 1992, Bulletin of the Earthquake Research Institute of the University of Tokyo (in Japanese), 68, 23-70.

Dominey-Howes, D., Dengler, L., Dunbar, P., Kong, L., Fritz, H., Imamura, F., McAdoo, B., Satake, K., Yalciner, A., Yamamoto, M., Yulianto, E., Koshimura, S., and Borrero, J. (2012). International Tsunami Survey Team (ITST) Post- Tsunami Survey Field Guide. 2nd Edition. UNESCO-IOC, Paris.

Gica E.M., Spillane, M., Titov, V.V., Chamberlin, C., and Newman, J.C. (2008) Development of the forecast propagation of the forecast propagation database for NOAA's Short-term Inundation Forecast for Tsunamis (SIFT), NOAA Tech. Memo OAR PMEL-139, 89 pp.

Hill, E, Borrero, J., Huang, Z., Qiu, Q., Banerjee, P., Natawidjaja, D., Elosegui, P., Fritz, H., Pranantyo, I., Li, L., Macpherson, K., Skanavis, V., Synolakis, C., and Sieh, K. (2012) The 2010 Mw 7.8 Mentawai earthquake: Very shallow source of a rare tsunami earthquake determined from tsunami field survey and near-field GPS. Journal of Geophysical Research, Vol 117, B06402, doi:10.1029/2012JB009159.

Kanamori, H. (1972) Mechanism of tsunami earthquakes, Phys. Earth Planet. Int., 6, 346-359.
Polet, J. and Kanamori, H. (2000) Shallow subduction zone earthquakes and their tsunamigenic potential, Geophys. J. Int., 142, 684-702.

Kanamori, H. and Kikuchi, M. (1993) The 1992 Nicaragua earthquake: a slow tsunami earthquake associated with subducted sediments. Nature, 361, 714- 716.

Newman, A.V., and Okal, E.A. (1998) Teleseismic estimates of radiated seismic energy: The E/M0 discriminant for tsunami earthquakes, J. Geophys. Res., 103, 26885-26898.

Newman, A. V., G. Hayes, Y. Wei, and J. Convers (2011), The 25 October 2010 Mentawai tsunami earthquake, from real-time discriminants, finite- fault rupture, and tsunami excitation, Geophys. Res. Lett., 38, L05302, doi:10.1029/2010GL046498.

Satake, K., Bourgeois, J., Abe, K., Abe, K., Tsuji, Y., Immura, F., Iio, Y., Katao, H., Noguera, E., and Estrada, F. Tsunami Field Survey of the 1992 Nicaragua Earthquake, Eos: Trans. Am. Geophys. Un. 74,13, pp145, 156-157.

Synolakis, C.E. & Okal, E.A., 2005. 1992–2002: Perspective on a decade of posttsunami surveys, in: Tsunamis: Case studies and recent develop- ments, ed. K. Satake, Adv. Nat. Technol. Hazards, 23:1–30.

Titov, V., and F. I. González (1997), Implementation and testing of the Method of Splitting Tsunami (MOST) model, NOAA Tech. Memo. ERL PMEL!112 (PB98!122773), 11 pp., Pac. Mar. Environ. Lab., NOAA, Seattle, Wash.

Wikipedia contributors, "El Salvador," Wikipedia, The Free Encyclopedia, http://en.wikipedia.org/w/index.php?title=El_Salvador&oldid=523734824 (accessed November 21, 2012).

ISSN 8755-6839

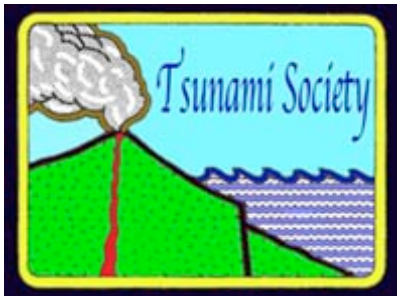

SCIENCE OF **TSUNAMI HAZARDS**

Journal of Tsunami Society International

Volume 34 **Number 4** **2015**

TSUNAMI SOCIETY INTERNATIONAL, 1741 Ala Moana Blvd. #70, Honolulu, HI 96815, USA.

WWW.TSUNAMISOCIETY.ORG